1 Supporting Information for "Unimolecular Reactions of Peroxy Radicals Formed in the Oxidation

2 of α-pinene and β-pinene by Hydroxyl Radicals"

3

4 Lu Xu[†], Kristian H. Møller[§], John D. Crounse[†], Rasmus V. Otkjær[§], Henrik G. Kjaergaard[§], Paul

5 O. Wennberg[†,⊥]

6 [†]Division of Geological and Planetary Sciences, California Institute of Technology, Pasadena,

7 California 91125, United States

8 [§]Department of Chemistry, University of Copenhagen, Universitetsparken 5, DK-2100,

9 Copenhagen Ø, Denmark

10 [⊥]Division of Engineering and Applied Science, California Institute of Technology, Pasadena,

11 California 91125, United States

12

Table of Contents

S1. Peak identification of α-pinene and β-pinene hydroxy nitrates

The structural assignment of α-pinene and β-pinene hydroxy nitrate isomers is achieved by the collection of several chromatograms. Firstly, the ring-opened HNs (i.e., 3-OH,8-ONO$_2$ for α-pinene and 1-OH,8-ONO$_2$ for β-pinene) are identified by adding O$_3$ to the chamber after photooxidation. The ring-opened HNs are unsaturated and thus react with O$_3$ while the ring-retained HN isomers are saturated and will not do so. After the photooxidation ceases, we remove the chamber content through a cold trap (i.e., 6.5 m ¼ inch PFA tubing submerged in -60°C isopropanol + liquid nitrogen bath). The oxidation products are trapped, but volatile compounds including precursor hydrocarbon, NO, NO$_2$ are not. Then, we remove the tubing from the trap and use a flow of zero air to send the trapped analytes back to chamber. 2-4 ppmv O$_3$ is added to chamber using an O$_3$ generator. We also inject approximately 90 ppmv cyclohexane, which serves as an OH scavenger. As shown in Figure S 1, the last peaks for both monoterpenes disappeared after O$_3$ addition, indicating that they are the ring-opened HNs.

The HNs with the –ONO$_2$ group on the less-substituted carbon (2-OH,3-ONO$_2$ for α-pinene and 2-OH,1-ONO$_2$ for β-pinene) are identified from NO$_3$ radical oxidation experiments. This approach is based on the assumption that NO$_3$ radicals react with alkenes by primarily adding to the less-substituted olefinic carbon[1]. Oxygen adds to the alkyl radical and these RO$_2$ react with other RO$_2$ to produce hydroxy nitrate (Scheme S 3). We perform NO$_3$ oxidation experiments by mixing ~200ppb NO and ~300ppb O$_3$ in an 800 L chamber, waiting for 1 hr to produce NO$_3$ and N$_2$O$_5$, and injecting about 80 ppbv α-pinene or β-pinene. The chromatograms of HNs from NO$_3$ oxidation experiments are shown in Figure S 2. For both α-pinene and β-pinene, only one peak is resolved from NO$_3$ oxidation experiments and the retention time of this peak matches that of the first in OH oxidation experiments.

The remaining peak in the OH oxidation is identified based on previous finding that the retention order for HNs with similar structures is generally tertiary –OH, secondary –OH, and then primary –OH for the same GC column [2]. This observation has a plausible rational as the primary –OH likely has stronger interaction with GC column than secondary or tertiary OH due to less shielding effects. Thus, the second peak in the α-pinene chromatogram is assigned to 3-OH,2-ONO$_2$, which has a secondary –OH and elutes later than 2-OH,3-ONO$_2$ with a tertiary –OH. Similarly, the second peak in the β-pinene chromatogram is assigned to 1-OH,2-ONO$_2$. We further

56　verify the structural assignment of HN peaks by comparing the chromatograms between α-pinene

57　and β-pinene using the same GC temperature profile (Figure S 3). α-pinene 3-OH,2-ONO$_2$ elutes

58　between β-pinene 2-OH,1-ONO$_2$ and 1-OH,2-ONO$_2$, which is consistent with the rule of thumb

59　described above. The ring-opened HNs elute later than ring-retained HNs because the ring-opened

60　HNs are more elongated.

61　　　Each peak in the 1 m chromatogram represents one structural isomer of HNs, but each peak

62　includes more than one diastereoisomer. Theoretically, there are ten diastereoisomers for α-pinene

63　HNs and five for β-pinene HNs, as shown in Scheme S 2. These diasteroisomers can be better

64　separated using a 5 m Restek RTX-1701 GC column (Figure S 10). For example, all four ring-

65　retained β-pinene HNs are separated with a 5 m GC column. The first peak in α-pinene HNs with

66　1 m GC is separated into two peaks with 5 m GC. Not all ten diastereoisomers are separated for α-

67　pinene HNs, likely due to some diastereoisomers co-eluting. Despite of improved separation,

68　significant transmission loss of the ring-opened HN (i.e., the last peak) is observed in the 5 m GC.

69　Because the key information for determination of the RO$_2$ isomerization rate is the separation of

70　ring-opened HNs from ring-retained HNs (e.g., 3-OH,8-ONO$_2$ vs. 3-OH,2-ONO$_2$+2-OH,3-ONO$_2$

71　in the α-pinene system), all of which are adequately separately using 1 m GC, we focus our analysis

72　on the data produced using the 1 m GC column.

73　　　For α-pinene, the abundance of ring-retained HNs and ring-opened HN is determined by

74　summing up the chromatogram signal from 700-1050 s and 1050-1350 s, respectively, after

75　subtracting the sample background. For β-pinene, the second peak has an apparent tailing, which

76　interference with the signal of the third peak. We apply Lorentzian function to represent the tailing

77　of the second peak (i.e., 1150-1800 s), extrapolate the fitting, and subtract the fitted function from

78　the 1800-2500 s data (Figure S 11). The abundance of the ring-opened HN (i.e., the third peak) is

79　determined by summing up the corrected signal between 1800 and 2500 s. The abundance of the

80　ring-retained HNs is determined by summing up the signal between 500 s and 2500 s and then

81　subtracting the abundance of the third peak. The uncertainty in the isomer abundance mainly arises

82　from the extrapolation of the tail of the second peak. To characterize the uncertainty in ring-opened

83　HN/ring-retained HNs ratio caused by the extrapolation, we applied bootstrap analysis. In the

84　analysis, we randomly select the start point (within range 1100-1200 s) and stop point (within

85　range 1700-1800 s) of the Lorentzian fit and then calculate the isomer ratio of each bootstrap trial.

86   The 25th and 75th percentiles of 1000 trials are used to represent the uncertainty of isomer ratio,
87   which is within 12% of the median value.

88   To further separate the structural isomers of the α-pinene ring-retained HNs, we use a
89   deconvolution algorithm[3] to analyze the 1 m chromatograms. Four equal-width Gaussian functions
90   are fitted to the chromatogram signal from 700 to 1050 s, with two peaks representing the 3-OH,2-
91   ONO_2 and the other two peaks representing 2-OH,3-ONO_2. A representative chromatogram fitting
92   is shown in Figure S 12. For β-pinene, the four ring-retained HNs are clearly separated with 5 m
93   GC, so we use the 5 m GC to obtain the relative abundance of ring-retained HNs. For the
94   diastereoisomer pair of β-pinene 1-OH,2-ONO_2, the abundance of *syn* isomer is roughly 4 times
95   higher than that of *anti* isomer, assuming the same sensitivity towards both diastereoisomers. This
96   observation suggests that O_2 preferentially adds to 1-OH,R• from the less sterically hindered side
97   without the two methyl substituents on the four-membered ring.

98   The GC transmission efficiency of an analyte is determined by the ratio of total
99   chromatogram signal to the amount of analyte trapped in the GC (i.e., product of signal during
100   direct sampling from the bag and trapping time). In the experiments with >1000 ppbv NO when
101   all hydroxy nitrate isomers are produced, the GC transmission efficiencies of α-pinene and β-
102   pinene hydroxy nitrates are 79±4% and 99±5%, respectively. In the experiments with no additional
103   NO injection when only ring-retained hydroxy nitrates are produced, the GC transmission
104   efficiencies of α-pinene and β-pinene hydroxy nitrates are 86±5% and 100%, respectively. The
105   similar transmission efficiencies between experiments with different NO concentrations suggest
106   that the transmission efficiency is isomer-independent within each monoterpene.

107   Different GC temperature profiles are used, depending on monoterpenes and column length.

- α-pinene and 1m GC: -20°C, + 20°C min^{-1} until 50°C, then +3°C min^{-1} until 120°C, hold 3 min.
- α-pinene and 5m GC: 30°C, + 20°C min^{-1} until 80°C, hold 100 min, then +20°C min^{-1} until 150°C, hold 10 min.
- β-pinene and 1m GC: -20°C, + 20°C min^{-1} until 80°C, hold 25 min, then +10°C min^{-1} until 130°C, hold 15 min.
- β-pinene and 5m GC: 30°C, + 20°C min^{-1} until 110°C, hold 25 min, then +20°C min^{-1} until 150°C, hold 4 min.

S2. Relationship between the (ring-opened HN):(ring-retained HNs) ratio and RO$_2$ lifetimes

117   We utilize the ratio of the ring-opened HN relative to that of the ring-retained HNs to probe the

118   unimolecular reactions of ring-opened RO$_2$. Below, we use a mathematical derivation to illustrate

119   the relationship between the (ring-opened HN):(ring-retained HNs) ratio and RO$_2$ bimolecular and

120   unimolecular lifetimes. We use α-pinene 2-OH,3-ONO$_2$ as an example of ring-retained HN. α-

121   pinene 3-OH,8-ONO$_2$ is the ring-opened HN. In the absence of secondary chemistry, the

122   production rates of 3-OH,8-ONO$_2$ and 2-OH,3-ONO$_2$ at time t_i are defined in Eqn. S(1) and S(2).

123

$$\frac{d[3\text{-OH,8-ONO}_2]}{dt} = BR_{3\text{-OH,8-ONO2}} \times k_{RO_2+NO}[3\text{-OH,8-RO}_2][NO] \quad \text{Eqn. S(1)}$$

$$\frac{d[2\text{-OH,3-ONO}_2]}{dt} = BR_{2\text{-OH,3-ONO2}} \times k_{RO_2+NO}[2\text{-OH,3-RO}_2][NO] \quad \text{Eqn. S(2)}$$

124   where the BR$_{3\text{-OH,8-ONO2}}$ and BR$_{2\text{-OH,3-ONO2}}$ are the branching ratio to produce organic nitrate from

125   RO$_2$+NO.

126   The time-rate-of-change of the two RO$_2$ at time t_i, in the absence of RO$_2$ + RO$_2$ chemistry

127   (reasonable assumption given the low VOC concentration in this study) can be described by Eqn.

128   S(3) and S(4)

129

$$\frac{d[3\text{-OH,8-RO}_2]}{dt} = Y_{3\text{-OH,8-RO}_2} \times k_{\alpha p+OH}[\alpha\text{-pinene}][OH] - k_{RO_2+NO}[3\text{-OH,8-RO}_2][NO] - k_{RO_2+HO_2}[3\text{-OH,8-RO}_2][HO_2] - k_{unimolecular}[3\text{-OH,8-RO}_2] \quad \text{Eqn. S(3)}$$

$$\frac{d[2\text{-OH,3-RO}_2]}{dt} = Y_{2\text{-OH,3-RO}_2} \times k_{\alpha p+OH}[\alpha\text{-pinene}][OH] - k_{RO_2+NO}[2\text{-OH,3-RO}_2][NO] - k_{RO_2+HO_2}[2\text{-OH,3-RO}_2][HO_2] \quad \text{Eqn. S(4)}$$

130   where, Y$_{3\text{-OH,8-RO2}}$ and Y$_{2\text{-OH,3-RO2}}$ are the yields of corresponding RO$_2$, k$_{\alpha p+OH}$, k$_{RO2+NO}$, k$_{RO2+HO2}$,

131   k$_{unimolecular}$ are the rate coefficients for α-pinene+OH, RO$_2$+NO, RO$_2$+HO$_2$, and RO$_2$ unimolecular

132   reactions, respectively. We assume that k$_{RO2+NO}$ and k$_{RO2+HO2}$ are isomer independent and all the

133   branching ratios and RO$_2$ yields are constants.

134   The steady state concentration of RO$_2$ can be expressed by:

135

$$[3\text{-OH,8-RO}_2] = \frac{Y_{3\text{-OH,8-RO}_2} \times k_{\alpha p+OH}[\alpha\text{-pinene}][OH]}{k_{RO_2+NO}[NO] + k_{RO_2+HO_2}[HO_2] + k_{unimolecular}} \quad \text{Eqn. S(5)}$$

$$[2\text{-OH,3-RO}_2] = \frac{Y_{2\text{-OH,3-RO}_2} \times k_{\alpha p+OH}[\alpha\text{-pinene}][OH]}{k_{RO_2+NO}[NO] + k_{RO_2+HO_2}[HO_2]} \quad \text{Eqn. S(6)}$$

136   Substituting Eqn. S(5) and S(6) into the ratio between Eqn. S(1) and S(2), we get

137

$$\frac{\dfrac{d[3\text{-OH},8\text{-ONO}_2]}{dt}}{\dfrac{d[2\text{-OH},3\text{-ONO}_2]}{dt}} = \frac{BR_{3\text{-OH},8\text{-ONO2}}}{BR_{2\text{-OH},3\text{-ONO2}}} \times \frac{[3\text{-OH},8\text{-RO}_2]}{[2\text{-OH},3\text{-RO}_2]}$$

$$= \frac{BR_{3\text{-OH},8\text{-ONO2}}}{BR_{2\text{-OH},3\text{-ONO2}}} \times \frac{Y_{3\text{-OH},8\text{-RO}_2}}{Y_{2\text{-OH},3\text{-RO}_2}} \times \frac{k_{RO_2+NO}[NO]+k_{RO_2+HO_2}[HO_2]}{k_{RO_2+NO}[NO]+k_{RO_2+HO_2}[HO_2]+k_{unimolecular}} \quad \text{Eqn. S(7)}$$

138   The RO$_2$ unimolecular lifetime $\tau_{unimolecular}$ (defined in Eqn. S(8)) is a constant, but the instantaneous

139   RO$_2$ bimolecular lifetime $\tau_{bimolecular,ins}$ (defined in Eqn. S(9)) changes over the duration of

140   experiments due to varying [HO$_2$] and [NO].

141

$$\tau_{unimolecular} = \frac{1}{k_{unimolecular}} \qquad\qquad \text{Eqn. S(8)}$$

$$\tau_{bimolecular,ins} = \frac{1}{k_{RO_2+NO}[NO]_{t_i}+k_{RO_2+HO_2}[HO_2]_{t_i}} \quad \text{Eqn. S(9)}$$

142   Substitute Eqn. S(8) and S(9) into Eqn. S(7), we get

143

$$\frac{\dfrac{d[3\text{-OH},8\text{-ONO}_2]}{dt}}{\dfrac{d[2\text{-OH},3\text{-ONO}_2]}{dt}} = \frac{BR_{3\text{-OH},8\text{-ONO2}}}{BR_{2\text{-OH},3\text{-ONO2}}} \times \frac{Y_{3\text{-OH},8\text{-RO}_2}}{Y_{2\text{-OH},3\text{-RO}_2}} \times \frac{\dfrac{1}{\tau_{bimolecular,ins}}}{\dfrac{1}{\tau_{bimolecular,ins}}+\dfrac{1}{\tau_{unimolecular}}}$$

$$= \frac{BR_{3\text{-OH},8\text{-ONO2}}}{BR_{2\text{-OH},3\text{-ONO2}}} \times \frac{Y_{3\text{-OH},8\text{-RO}_2}}{Y_{2\text{-OH},3\text{-RO}_2}} \times \frac{\tau_{unimolecular}}{\tau_{unimolecular}+\tau_{bimolecular,ins}} \quad \text{Eqn. S(10)}$$

144   By integrating Eqn. S(10) over the duration of the experiment, we get

145

$$\frac{\Delta[3\text{-OH},8\text{-ONO}_2]}{\Delta[2\text{-OH},3\text{-ONO}_2]} = \frac{BR_{3\text{-OH},8\text{-ONO2}}}{BR_{2\text{-OH},3\text{-ONO2}}} \times \frac{Y_{3\text{-OH},8\text{-RO}_2}}{Y_{2\text{-OH},3\text{-RO}_2}} \times \frac{\tau_{unimolecular}}{\tau_{unimolecular}+\tau_{bimolecular}} \quad \text{Eqn. S(11)}$$

146   where $\tau_{bimolecular}$ represents the average RO$_2$ bimolecular lifetime over the duration of the

147   experiment. Thus, by plotting $\dfrac{\Delta[3\text{-OH},8\text{-ONO}_2]}{\Delta[2\text{-OH},3\text{-ONO}_2]}$ as a function of $\tau_{bimolecular}$, we can calculate

148    $\tau_{unimolecular}$, which is $1/k_{unimolecular}$. In the actual analysis, the sum of two structural isomers of the

149   ring-retained HNs (2-OH,3-ONO$_2$ and 3-OH,2-ONO$_2$) is used.

150   To calculate $\tau_{bimolecular}$, we estimate the concentrations of NO and HO$_2$ from modified

151   Master Chemical Mechanims (MCM)[4]. The major modifications we make are (1) updating the

152   nitrate branching ratio based on measurements (Section S6) and (2) updating the ring-opening

153   fraction of activated alkyl radical based on RO-CCSD(T)-F12a/VDZ-F12//ωB97X-D/aug-cc-

154   pVTZ calculation (Section S5.3). We also include the unimolecular reactions of ring-opened RO_2.

155   Because a myriad of products is produced from the unimolecular reactions, we assume the

156   unimolecular reactions of ring-opened RO_2 produce a generic RO_2 in the model. As this

157   assumption conserves the RO_2 concentration, unimolecular reactions have little effect on the NO

158   and HO_2 concentrations.

159   The measured concentrations of NO, hydrocarbon (α-pinene or β-pinene), and CH_3ONO

160   are used as initial concentrations in MCM. The measured spectral radiance of the chamber light is

161   input in MCM, but is adjusted until the modeled hydrocarbon decay agrees with measurements.

162   The modeled NO and HO_2 concentrations over the course of photooxidation are used to calculate

163    $\tau_{bimolecular,ins}$. As the NO and HO_2 concentrations change over time, we calculate an average

164    $\tau_{bimolecular}$ by weighting the $\tau_{bimolecular,ins}$ by the instantaneous α-pinene consumption amount in each

165   simulation time step. The uncertainty in $\tau_{bimolecular}$ is represented by the range of $\tau_{bimolecular,ins}$ from

166   the beginning to the end of photooxidation. As shown in Figure 2, the uncertainty increases with

167   longer $\tau_{bimolecular}$.

168   For experiments with no initial NO injection (i.e., Experiments 6 and 13 in Table S 1), we

169   estimate the concentrations of NO and HO_2 by following the procedures in Crounse et al. and Teng

170   et al. [5-6] In brief, the HO_2 concentration is calculated from the measured production rate of H_2O_2

171   and rate coefficient for the HO_2+HO_2. The NO concentration is inferred from HO_2 concentration

172   and the measured production rates of hydroxy nitrate and hydroxy hydroperoxides. The calculated

173    $\tau_{bimolecular}$ from this method are 3.8 s and 8.9 s for Experiments 6 and 13, respectively, which agree

174   well with the values estimated using MCM, which are 5.7 s and 9.5 s, respectively.

175   We also calculate $\tau_{bimolecular}$ using the default nitrate branching ratio in MCM. Figure S 13

176   compares the $\tau_{bimolecular}$ calculated by using updated and default nitrate branching ratio. The

177   difference is negligible. This is mainly because NO concentration is close to its initial

178   concentration, as a result of small OH exposure in the experiments.

179

180

S3. Computational approach

S3.1 Dipole moments and polarizabilities

Dipole moments and polarizabilities are calculated for (1) the 15 different hydroxy nitrates formed by addition of OH, O_2 and subsequently NO to α-pinene and β-pinene (Table S 2); (2) the 15 different hydroxy hydroperoxides formed by addition of OH, O_2 and reaction with HO_2 to α-pinene and β-pinene (Table S 3); (3) glycolaldehyde used as a calibration reference and endoperoxide ketoaldehyde (P2 in Scheme 3) formed later in the α-pinene oxidation (Table S 4).

The dipole moments and polarizabilities are calculated using an approach previously employed [7-9]. Briefly, the structures are drawn and a conformational sampling is carried out using MMFF in Spartan '14 [10-16]. All resulting structures are optimized at the B3LYP/6-31+G(d) level in Gaussian 16, rev. A.03 [17-22] with default convergence criteria and integration grid. All unique structures within 15 kJ/mol in electronic energy of the lowest-energy conformer are further optimized using B3LYP/cc-pVTZ [23]. The average dipole moment of each structure is calculated as a Boltzmann weighted average of the conformers at 298 K. The polarizability is calculated only for the lowest-energy conformer of each isomer, as it varies by less than 3% between conformers of the same compound. The calculated CIMS sensitivities of a few test compounds using the augmented aug-cc-pVTZ basis set change by less than 4 % compared to the values obtained using cc-pVTZ, see Table S 5.

S5.2 The rate coefficients of unimolecular reactions

The rate coefficients of the unimolecular reactions of the peroxy radicals are calculated using the approach by Møller et al. [24] For the reactant and transition state, a conformational sampling is carried out in Spartan'14 or '16 using MMFF with a neutral charge enforced on the radical center [10-16, 25]. For the reactant, the input is a geometry simply drawn. For the transition state, the conformational sampling is preceded by an optimization using B3LYP/6-31+G(d) in Gaussian 16, rev. A.03, which is then used as input for the conformer search [17-22]. Furthermore, during the conformational sampling of the transition state, three bond lengths are constrained to the values from the optimized TS: For the H-shifts, the peroxy O-O length, the O···H length and the H···C (or H···O) length and for the endoperoxide formations, the peroxy O-O length, the length of the O···C bond forming and the length of the C-C bond going from a double to a single bond [24]. The structures resulting from the conformer searches are optimized using B3LYP/6-31+G(d) in

Gaussian 16. For the transition states, the free transition state optimization is preceded by a constrained optimization using the same constraints as for the conformational sampling. Conformers within $1 \cdot 10^{-5}$ hartree and $1.5 \cdot 10^{-2}$ D in energy and dipole moment, respectively, of each other are identified as duplicates and only one is kept.[24] All unique conformers with electronic energies within 2 kcal/mol of the lowest-energy conformer are further optimized at the ωB97X-D/aug-cc-pVTZ level of theory [23, 26-27]. In Møller et al., a cut-off based on electronic energy at this level was found to be suitable.

For the lowest-energy conformer (based on electronic plus zero-point vibrational energy (ZPVE)) at this level, an RO-CCSD(T)-F12a/VDZ-F12//ωB97X-D/aug-cc-pVTZ (abbreviated F12) single-point calculation is done using Molpro 2012 [28-34]. This has not been done for H-shifts that abstract from an OH group, and thus the rate coefficients for these are expected to have a slightly higher uncertainty. All F12 calculations have T1 values lower than 0.025, which is well below the value of 0.04 generally accepted for open-shell systems[35-37]. For the reactions of A1, Gaussian 09, rev. D.01 was used instead of Gaussian 16, but the approach was otherwise identical. For both the calculations in Gaussian 09 and 16, the default convergence criteria were used along with the ultrafine integration grid, which is the default in Gaussian 16. In Møller et al., it was found that the default optimization convergence criteria in Gaussian 09 yielded rate coefficients within 1 % of those obtained using "opt=verytight".

From the B3LYP/6-31+G(d) optimized TS structure of the conformer corresponding to the lowest-energy conformer (based on electronic plus ZPVE) at the ωB97X-D/aug-cc-pVTZ level, an IRC is calculated at the B3LYP/6-31+G(d) level using the "calcall" keyword. The IRC end-points are optimized first using B3LYP/6-31+G(d) and subsequently using ωB97X-D/aug-cc-pVTZ. Finally, an F12 single-point calculation is done. Eckart tunneling coefficients are calculated in MATLAB R2016b using barrier heights with F12 electronic energies and ωB97X-D/aug-cc-pVTZ ZPVE and the imaginary frequency of the TS calculated using ωB97X-D/aug-cc-pVTZ [38-39].

Reaction rate coefficients, k, are calculated using multi-conformer transition state theory (MC-TST) [24, 40-42]:

$$k = \kappa \frac{k_B T}{h} \cdot \frac{\sum_i^{All\ TS\ conf.} \exp\left(-\frac{\Delta E_i}{k_B T}\right) Q_{TS_i}}{\sum_j^{All\ R\ conf.} \exp\left(-\frac{\Delta E_j}{k_B T}\right) Q_{TS_j}} \cdot \exp\left(-\frac{E_{TS} - E_R}{k_B T}\right) \quad \text{Eqn. S(12)}$$

240   where k_B is the Boltzmann constant, T is the absolute temperature, h is Planck's constant, the sums

241   are over all transition state and reactant conformers, respectively and sum their partition functions

242   (Q) Boltzmann weighted by their energy calculated relative to the lowest-energy conformer. The

243   final term has the energy difference between the lowest-energy TS and reactant conformers, the

244   barrier height. The barrier heights are calculated using F12 electronic energies with ωB97X-D/aug-

245   cc-pVTZ ZPVE and ωB97X-D/aug-cc-pVTZ is used for the partition functions and relative energy

246   between conformers. The partition functions are calculated using the harmonic oscillator rigid

247   rotor approximation. All reaction rate coefficients are calculated at 298.15 K. Rate coefficients

248   calculated at this level are given in Table S 6 and Table S 7.

249   Rate coefficients calculated similarly, but using ωB97X-D/aug-cc-pVTZ for all values

250   including the electronic energy are given in Table S 8 and Table S 9. The rate coefficients of three

251   unimolecular channels (i.e., 1,5 H-shift, 1,6 H-shift, and 6-membered endoperoxide formation) of

252   A1 using ωB97X-D/aug-cc-pVTZ were reported in Berndt et al. [43]

253   As an approach for eliminating slow reactions, MC-TST reaction rate coefficients were

254   calculated following the B3LYP/6-31+G(d) calculations for all reactions (Table S 10 and Table S

255   11). For these reactions, tunneling was estimated from the barrier height (energy difference

256   between lowest-energy reactant and TS conformers) and assuming a thermoneutral reaction (i.e. a

257   symmetrical barrier) [44]. The Eckart tunneling coefficient is thus calculated with same forward and

258   reverse barriers, which are equal to the reaction barrier and the imaginary frequency of the lowest-

259   energy (E_e+ZPVE) conformer at the B3LYP/6-31+G(d) level. Compared to the more formally

260   correct approach of using the IRC end-points for the tunneling barriers, this is expected to represent

261   an upper limit for the Eckart tunneling correction (with a given imaginary frequency) [24]. Firstly,

262   the reaction barrier is the upper limit for the forward Eckart barrier and likely the IRC connects to

263   a higher-energy reactant conformer [24]. Secondly, the peroxy radical H-shift reactions are generally

264   energetically uphill, which means that the reverse IRC barrier is usually lower than the forward.

265   For the unimolecular reactions of B5 (the ring-opened β-pinene hydroxy peroxy radical), we show

266   that the Eckart tunneling coefficients calculated using this approach do indeed represent upper

267   limits for the B3LYP Eckart tunneling coefficient, see Table S 12. The use of upper limit tunneling

268   coefficients for the MC-TST B3LYP reaction rate coefficients allows to more confidently

269   eliminate slow reactions at this level. Reactions with rate coefficients below $5 \cdot 10^{-3}$ s^{-1} were not

270   considered at a higher level. However, for a few reactions with rate coefficient below this value,

271   higher-level reaction rate coefficients were calculated to validate the value of the cut-off.

272   **S5.3 Calculations on the ring-opening fraction of hydroxy alkyl radicals**

273   Conformational sampling and subsequent computational steps were done as described in the

274   approach by Møller et al. (see above) [24] using Gaussian 09 for the DFT calculations. For the RRKM

275   simulations, the electronic energy of the species important for the simulation (the free reactants,

276   the hydroxy alkyl radicals and the ring-opening TS) are calculated using RO-CCSD(T)-

277   F12a/VDZ-F12//ωB97X-D/aug-cc-pVTZ (abbreviated F12) while all other values are calculated

278   using ωB97X-D/aug-cc-pVTZ. For reference, the canonical (for the species without excess energy)

279   MC-TST reaction rate coefficients for the ring-opening reactions are also calculated using the

280   approach described above (but these values are not used in the simulation). The canonical MC-

281   TST reaction rate coefficients do not include a tunneling correction due to the large mass being

282   transferred (tunneling coefficient estimated to be less than a factor of 2). The Eckart tunneling

283   correction is used in the simulations.

284   RRKM modelling is done using the Master Equation Solver for Multi-Energy well

285   Reactions (MESMER) for the lowest-energy conformers (MESMER uses only a single

286   conformer)[45]. For the simulations, the following parameters are used:

287   • $k(\alpha\text{-pinene} + OH, 300\text{ K}) = 6.08 \cdot 10^{-11}$ cm^{-3} molecule^{-1} s^{-1} , [46]

288   • $k(\beta\text{-pinene} + OH, 300\text{ K}) = 7.72 \cdot 10^{-11}$ cm^{-3} molecule^{-1} s^{-1} , [46]

289   • $[OH] = 1 \cdot 10^{6}$ molecules cm^{-3} corresponding to the estimated global average value.

290   • $k(R\cdot + O_2) = 14 \cdot 10^{-12}$ cm^{-3} molecule^{-1} s^{-1} [47]. This is the value for cyclohexanyl + O$_2$ and

291   corresponds to a pseudo-first order rate coefficient of $7.2 \cdot 10^{7}$ s^{-1}. The exact rate of this

292   addition is not important for the simulation, as long as it is significantly faster than the rate

293   of ring-opening for the thermalized radicals (10^{2}-10^{3} s^{-1}, see Table S 15) and slower than

294   the excess energy reaction (~10^{10} s^{-1}) [48].

295   • Exponential energy decay with energy transfer per collision (ΔE_{down}) = 225 cm^{-1}. This

296   value is based on values for similar simulations with N$_2$ as the bath gas [49-50].

297   • Lennard-Jones parameters for the pinene-derived species: $\sigma = 6.5$ Å, $\varepsilon/k_b = 600$ [50].

298   • Bath gas = N$_2$ ($\sigma = 3.919$ Å, $\varepsilon/k_b = 91.85$) [51]

299   • P = 760 Torr, T = 298.15 K

300 • Grain size $= 100$ cm^{-1} and energy grain span above the highest stationary point $= 50k_BT$.

301   The system being modelled is illustrated for β-pinene in Figure S 14 for exemplification.
302 As can be seen, the hydroxy alkyl radical is formed with almost 30 kcal/mol excess energy and the
303 barrier for ring-opening is about 13 kcal/mol. As shown in Table S 15, the energetics are very
304 similar for all three systems. As expected from the comparable energetics of the three systems, the
305 calculated amount modelled to ring open is very similar for all three at around 30-50 % (Table S
306 15). The difference between α-pinene and β-pinene is within the uncertainty of the modelling.
307 Very similar results are obtained when all values are calculated using ωB97X-D/aug-cc-pVTZ
308 (Table S 16), but with slightly higher barriers leading to slightly lower yields of the ring-opened
309 product.

310   To assess the sensitivity of the model, the analysis was redone for the systems where the
311 barrier for ring-opening had either been decreased or increased by 1 kcal/mol. As shown in Table
312 S 17, this roughly changes the fraction ring-opening by a factor of two in either direction. We also
313 test the sensitivity of the model towards the energy being transferred per collision (ΔE_{down}), as
314 shown in Table S 18. The results in the table confirm that the ring-opening is driven by the excess
315 energy in the hydroxy alkyl radical, as decreasing the energy transfer per collision increases the
316 yield of ring-opened product and vice versa.

317

S4. Kinetic box model to simulate the relationship between the (ring-opened HN):(ring-retained HNs) ratio and RO$_2$ lifetimes

To obtain the distribution of HN isomers under certain $\tau_{bimolecular}$, we solve the time-dependent set of ordinary differential equations (ODEs) for the following systems, which include the oxidation reactions of α-pinene depicted in Scheme 1.

$$\frac{d[\alpha\text{-pinene}]}{dt} = -k_{\alpha p + OH} \times [\alpha\text{-pinene}] \times [OH]$$

$$\frac{d[2\text{-OH,3-RO}_2]}{dt} = Y_{2\text{-OH,3-RO}_2} \times k_{\alpha p + OH}[\alpha\text{-pinene}] \times [OH] - k_{RO_2 + NO}[2\text{-OH,3-RO}_2] \times [NO]$$

$$\frac{d[3\text{-OH,2-RO}_2]}{dt} = Y_{3\text{-OH,2-RO}_2} \times k_{\alpha p + OH}[\alpha\text{-pinene}] \times [OH] - k_{RO_2 + NO}[3\text{-OH,2-RO}_2] \times [NO]$$

$$\frac{d[3\text{-OH,8-RO}_2]}{dt} = Y_{3\text{-OH,8-RO}_2} \times k_{\alpha p + OH}[\alpha\text{-pinene}] \times [OH] - k_{RO_2 + NO}[3\text{-OH,8-RO}_2] \times [NO] - k_{unimolecular}[3\text{-OH,8-RO}_2]$$

$$\frac{d[2\text{-OH,3-ONO}_2]}{dt} = BR_{2\text{-OH,3-ONO}_2} \times k_{RO_2 + NO}[2\text{-OH,3-RO}_2] \times [NO]$$

$$\frac{d[3\text{-OH,2-ONO}_2]}{dt} = BR_{3\text{-OH,2-ONO}_2} \times k_{RO_2 + NO}[3\text{-OH,2-RO}_2] \times [NO]$$

$$\frac{d[3\text{-OH,8-ONO}_2]}{dt} = BR_{3\text{-OH,8-ONO}_2} \times k_{RO_2 + NO}[3\text{-OH,8-RO}_2] \times [NO]$$

The symbols have the same meaning as those in section S2. To achieve the same OH exposure as experiments, we assume a constant OH concentration (2×10^6 molec cm^{-3}) and interval of integration (1000 s). Our procedure to obtain the optimized $k_{unimolecular}$ is the following. First, by solving the set of ODEs under fixed NO concentration and $k_{unimolecular}$, we obtain the (ring-opened HN):(ring-retained HNs) ratio at fixed $\tau_{bimolecular}$ and $k_{unimolecular}$. Second, under a fixed $k_{unimolecular}$ but varying NO concentration, we obtain the relationship between (ring-opened HN):(ring-retained HNs) ratio and $\tau_{bimolecular}$. Third, we vary $k_{unimolecular}$ to obtain different relationships between (ring-opened HN):(ring-retained HNs) ratio and $\tau_{bimolecular}$. Finally, we compare the simulated relationships under varying $k_{unimolecular}$ with measurements to determine the optimized $k_{unimolecular}$. We determine the upper and lower bounds of the $k_{unimolecular}$ in a way that 80% of the experimental data points are placed on the same side of the simulated curve. The upper and lower bounds are used to calculate the average and the uncertainty range of $k_{unimolecular}$ assuming symmetric uncertainties.

S5. Yields of α-pinene and β-pinene hydroxy nitrates

We estimate the instrumental sensitivity (c_x) towards HNs based on the ion-molecular collision rate coefficients (k_x). The rate coefficients are calculated from the dipole moment (μ) and polarizability (α) using the empirical approach developed by Su et al. [52]. The μ and α for all 10 α-pinene HN isomers and 5 β-pinene HNs are calculated using Density Function Theory (DFT) B3LYP/cc-pVTZ (Section S3.1) and are listed in Table S 2.

We relate the k_x to c_x by using glycoaldehyde as a calibration reference

$$c_x = \frac{k_x}{k_{glycoaldehyde}} \times c_{glycoaldehyde}$$

where $k_{glycoaldehyde}$ is 2.0×10^{-9} cm^3 molec^{-1} s^{-1} using the empirical approach by Su et al. [52] and $c_{glycoaldehyde}$ is experimentally determined to be 1.5×10^{-4} ncts pptv^{-1} where ncts (normalized counts) is the observed ion count rate divided by the sum of the count rates for $^{13}CF_3O^-$ and $^{13}CF_3O^- \cdot H_2O$.

The signal of an individual HN isomer is calculated by multiplying the total signal of all HNs during direct sampling by the corresponding GC fractional abundances. Isomer-specific sensitivity is applied to convert the signal to mixing ratio. The molar yield of a HN isomer is the change in HN concentration over the consumed parent hydrocarbon. The overall yield of all HN isomers is the summation over all individual isomers. We quantify the overall yields of HN to be $3.3 \pm 1.5\%$ and $6.4 \pm 2.1\%$ for α-pinene and β-pinene, respectively. The mean value is obtained from the average of five experiments with initial NO concentration above 1000 ppbv. The uncertainty is calculated by propagating the standard deviations of HN yields from five experiments (15% for α-pinene and 6% for β-pinene), the instrumental sensitivity uncertainty (~30%), initial hydrocarbon concentration uncertainty (~10%), secondary loss (~5%), and vapor wall loss (~2%). The secondary loss of HN by reaction with OH [53] is negligible (<5%) because of the low OH exposure in the experiments (roughly 2×10^9 and 1×10^9 molecules cm^{-3} s for α-pinene and β-pinene experiments, respectively). The measured wall loss rate constant for HN is 1×10^{-5} s^{-1}. In 30 min (i.e., the oxidation time in experiments to quantify the hydroxy nitrate yield), 2% of gas-phase hydroxy nitrate is lost to wall. To evaluate the sample loss in the 2 m Teflon sampling line, we increased the sampling flow rate from 1 LPM to 2 LPM. No discernable change in hydroxy nitrate concentration was observed, suggesting negligible loss in sampling line.

366   We note that the overall yield reported here only accounts for the first generation gas phase
367 HNs. Considering that less than 10 ppbv hydrocarbon is oxidized, the fraction of HNs in the
368 particle phase is expected to be small. According to Eddingsaas et al. [54] who used similar initial α-
369 pinene concentration as our study, the SOA yield is ~5% when OH exposure is ~2×10^9 molec cm^{-}
370 ^{3} s. Thus, roughly 3 μg m^{-3} SOA is produced from the oxidation of 10 ppbv α-pinene. Bean et al.
371 reported that when OA concentration is below 40 μg m^{-3}, only 5–10% of α-pinene organic nitrates
372 are expected to partition to the particle phase [55]. Therefore, the effect of gas/particle partitioning
373 on our measured HNs yield is within 10%. To further test the effect of gas/particle partitioning on
374 the gas phase HN yields, we perform experiments with ~300ppbv initial VOC and oxidize
375 ~30ppbv VOC to keep the OH exposure the same as low VOC experiments. The HNs yields are
376 not statistically significant between high and low VOC experiments (3.2±1.5% when Δα-pinene <
377 10 ppbv vs. 3.4±1.5% when Δα-pinene = ~30ppbv; 6.3±2.1% when Δβ-pinene < 10ppbv vs.
378 6.9±2.3% when Δβ-pinene = ~30ppbv), suggesting a minor effect of gas/particle partitioning on
379 HNs yield. From the high vs. low VOC experiments, we also find that the gas/particle partitioning
380 has small effect on the distribution of HN isomers (Figure S 15).

381   In α-pinene short $\tau_{bimolecular}$ experiments, we observe CIMS signals at a number of even
382 masses (Table S 20). If we assume that the compounds appearing at even mass are nitrogen-
383 containing organic compounds and assume that these compounds have the same sensitivity as the
384 average of all α-pinene hydroxy nitrate isomers, we estimate an overall yield of organic nitrates to
385 be 9%. This roughly estimated yield is half of the total nitrates yield quantified by FT-IR in an
386 earlier study (18%±9%) [56]. However, we note that the alkyl nitrates produced from OH abstraction
387 channel are detected by FTIR, but not by CF_3O^- CIMS, which partly contributes to the discrepancy.
388 The uncertainties in instrumental sensitivity also can largely influence the comparison. Following
389 the same analysis as α-pinene, the overall yield of organic nitrates is estimated to be 11% for β-
390 pinene.

391 **S6. Discussion of branching ratios and associated uncertainties in α-pinene oxidation.**

392 The formation pathway of α-pinene HNs and co-products is shown in Scheme S 7. The branching
393 ratio for each reaction step is discussed below. BR in this study is defined as the ratio of the rate
394 constant for a particular product of a reaction to the rate constant for the total set of possible
395 products[57].

396   1) BR_{OH_add} represents the fraction of α-pinene + OH that proceeds via addition to the double
397   bond. Early theoretical studies estimate that BR_{OH_add} is 90% based on structure-activity
398   relationships [58-59].

399   2) $BR_{OH\_less\_sub}$ represents the fraction of OH adding onto the less-substituted olefinic carbon.
400    $BR_{OH\_less\_sub}$ is equivalent to BR_{add_C3} in Scheme S 7 and BR_{add_C1} in Scheme S 8. These ratios have
401   not been experimentally constrained. The OH addition branching ratio for 2-methyl 2-butene,
402   which shares a similar substitutions around the C-C double bond with α-pinene, though does not
403   have the rigid constraints of a ring structure, is 69% : 31% as experimentally constrained in Teng
404   et al. [2] However, Peeters et al. suggested that the bicyclic ring structure may affect the substitution
405   effect and hence conjectured the branching ratio as 50% : 50%.

406   3) $BR_{ring\text{-}open}$ represents the ring-opening fraction of activated alkyl radicals. $BR_{ring\text{-}open}$ has
407   been extensively discussed in the main text. In brief, Peeters et al.[58] and our theoretical calculations
408   (F12 level) suggest $BR_{ring\text{-}open}$ to be 50% and 32%, respectively for 3-OH,2-R• from α-pinene +
409   OH.

410   4) BR_{RONO2} represents the nitrate branching ratio of RO_2 reaction with NO to form $RONO_2$
411   BR_{RONO2} is shown as "BR1-3" in Scheme S 7). An estimate of BR_{RONO2} for each RO_2 isomer can
412   be calculated from the measured yield of corresponding HN isomer and the branching ratios for
413   each step along HN formation pathway. Using 50% as the BR_{add_C2} (from Peeters et al. [58]) and 32%
414   as the $BR_{ring\text{-}open}$ (from our theoretical calculation), we calculate that the BR_{RONO2} is 3.1%, 0.7%,
415   and 10.8% for α-pinene 2-OH,3-RO_2, 3-OH,2-RO_2, and 3-OH,8-RO_2, respectively. Using the same
416   approach, we estimate that the BR_{RONO2} is 15.9%, 10.2%, and 1.7% for β-pinene 2-OH,1-RO_2, 1-
417   OH,2-RO_2, and 1-OH,8-RO_2, respectively. The widely ranging BR_{RONO2} for RO_2 with similar
418   structures is surprising and may indicate errors in the calculated branching ratios. For example,
419   BR_{RONO2} of α-pinene ring-opened peroxy radical, 3-OH,8-RO_2 (10.8%), is six times larger than
420   that of β-pinene ring-opened peroxy radical, 1-OH,8-RO_2 (1.7%).

421   Considering the large uncertainties in the above branching ratios, we suggest an alternative
422   constraint on them based on measured yield of hydroxy nitrate isomers. We assume that the ring-
423   opened tertiary RO_2 of both α-pinene and β-pinene have the same BR_{RONO2} (denoted as
424   "$BR_{RONO2,ring\text{-}open}$"). This assumption is reasonable as the ring-opened RO_2 of both terpenes share
425   very similar structure (i.e., tertiary RO_2 in the -$C(CH_3)_2OO$ group). Further, we assume that all the
426   β-hydroxy RO_2 have the same BR_{RONO2} (denoted as "$BR_{RONO2,\beta\text{-}OH}$"), following study by Teng et

427   al.[6] Based on these two assumptions, we can express the yields of six hydroxy nitrate isomers (α-

428   pinene and β-pinene combined) by propagating the branching ratio of each step as shown below,

429     $Y_{\alpha\text{-pinene 3-OH,8-ONO2}} = BR_{OH\_add} \times BR_{add\_C3} \times BR_{\alpha\text{-pinene,ring-open}} \times BR_{RONO2,ring\text{-open}}$

430     $Y_{\alpha\text{-pinene 3-OH,2-ONO2}} = BR_{OH\_add} \times BR_{add\_C3} \times (1 - BR_{\alpha\text{-pinene,ring-open}}) \times BR_{RONO2,\beta\text{-OH}}$

431     $Y_{\alpha\text{-pinene 2-OH,3-ONO2}} = BR_{OH\_add} \times (1 - BR_{add\_C3}) \times BR_{RONO2,\beta\text{-OH}}$

432     $Y_{\beta\text{-pinene 1-OH,8-ONO2}} = BR_{OH\_add} \times BR_{add\_C1} \times BR_{\beta\text{-pinene,ring-open}} \times BR_{RONO2,ring\text{-open}}$

433     $Y_{\beta\text{-pinene 1-OH,2-ONO2}} = BR_{OH\_add} \times BR_{add\_C1} \times (1 - BR_{\beta\text{-pinene,ring-open}}) \times BR_{RONO2,\beta\text{-OH}}$

434     $Y_{\beta\text{-pinene 2-OH,1-ONO2}} = BR_{OH\_add} \times (1 - BR_{add\_C1}) \times BR_{RONO2,\beta\text{-OH}}$

435   BR_{OH_add} is 0.9 as discussed above. BR_{add_C3} and BR_{add_C1} represent the branching ratio of OH

436   adding onto C3 and C1 in α-pinene and β-pinene, respectively. The yield of each hydroxy nitrate

437   isomer is measured in this study. BR_{add_C3}, BR_{add_C1}, $BR_{\alpha\text{-pinene,ring-open}}$, $BR_{\beta\text{-pinene,ring-open}}$, $BR_{RONO2,\beta\text{-}}$

438     $_{OH}$, and $BR_{RONO2,ring\text{-open}}$ are unknowns. By solving the system of equations (six equations and six

439   unknowns), we find that

440     $BR_{add\_C3} = 0.83$,

441     $BR_{add\_C1} = 0.88$,

442     $BR_{\alpha\text{-pinene,ring-open}} = 0.97$,

443     $BR_{\beta\text{-pinene,ring-open}} = 0.34$,

444     $BR_{RONO2,\beta\text{-OH}} = 0.092$,

445     $BR_{RONO2,ring\text{-open}} = 0.022$.

446   To evaluate how the assumption on BR_{RONO2} affects the $BR_{ring\text{-open}}$, we extend the approach

447   by implementing different constraints on BR_{RONO2}. For example, we assume that the ratio of

448   BR_{RONO2} for tertiary, secondary, and primary β-hydroxy RO_2 is 1.25: 1: 0.75 as suggested by

449   Wennberg et al.[60]. Now, the system contains eight equations and eight unknowns, as shown below.

450     $Y_{\alpha\text{-pinene 3-OH,8-ONO2}} = BR_{OH\_add} \times BR_{add\_C3} \times BR_{\alpha\text{-pinene,ring-open}} \times BR_{RONO2,ring\text{-open}}$

451     $Y_{\alpha\text{-pinene 3-OH,2-ONO2}} = BR_{OH\_add} \times BR_{add\_C3} \times (1 - BR_{\alpha\text{-pinene,ring-open}}) \times BR_{RONO2,\beta\text{-OH,3rd}}$

452     $Y_{\alpha\text{-pinene 2-OH,3-ONO2}} = BR_{OH\_add} \times (1 - BR_{add\_C3}) \times BR_{RONO2,\beta\text{-OH,2nd}}$

453     $Y_{\beta\text{-pinene 1-OH,8-ONO2}} = BR_{OH\_add} \times BR_{add\_C1} \times BR_{\beta\text{-pinene,ring-open}} \times BR_{RONO2,ring\text{-open}}$

454     $Y_{\beta\text{-pinene 1-OH,2-ONO2}} = BR_{OH\_add} \times BR_{add\_C1} \times (1\text{-}BR_{\beta\text{-pinene,ring-open}}) \times BR_{RONO2,\beta\text{-OH,3rd}}$

455     $Y_{\beta\text{-pinene 2-OH,1-ONO2}} = BR_{OH\_add} \times (1\text{-}BR_{add\_C1}) \times BR_{RONO2,\beta\text{-OH,1st}}$

456     $BR_{RONO2,\beta\text{-OH,1st}} = 0.75 \times BR_{RONO2,\beta\text{-OH,2nd}}$

457     $BR_{RONO2,\beta\text{-OH,3rd}} = 1.25 \times BR_{RONO2,\beta\text{-OH,2nd}}$

458   where $BR_{RONO2,\beta\text{-OH,1st}}$, $BR_{RONO2,\beta\text{-OH,2nd}}$, $BR_{RONO2,\beta\text{-OH,3rd}}$ represents the BR_{RONO2} for primary,

459   secondary, and tertiary β-hydroxy RO_2, respectively. Other symbols have the same meaning as in

460   previous equations.

461   By solving the new system of equations, we find that

462     $BR_{add\_C3} = 0.81,$

463     $BR_{add\_C1} = 0.82,$

464     $BR_{\alpha\text{-pinene,ring-open}} = 0.97,$

465     $BR_{\beta\text{-pinene,ring-open}} = 0.36,$

466     $BR_{RONO2,ring\text{-open}} = 0.023,$

467     $BR_{RONO2,\beta\text{-OH,1st}} = 0.061,$

468     $BR_{RONO2,\beta\text{-OH,2nd}} = 0.082,$

469     $BR_{RONO2,\beta\text{-OH,3rd}} = 0.10.$

470   Different assumptions have minor effect on $BR_{ring\text{-open}}$. More importantly, the $BR_{\alpha\text{-pinene,ring-}}$

471     $_{open}$ and $BR_{\beta\text{-pinene,ring-open}}$ are substantially different from the theoretical calculations. This has been

472   discussed in the main text.

473   From the above calculation, we find that $BR_{RONO2,\beta\text{-OH,3rd}}$ is about four times larger than

474     $BR_{RONO2,ring\text{-open}}$. This result is consistent with experimentally observed products distribution in β-

475   pinene system. From Figure 4b, it can be inferred that

476
$$\frac{\text{yield of endoperoxide hydroxy nitrate } (C_{10}H_{17}NO_6) \text{ at } \tau_{bimolecular} = 10 \text{ s}}{\text{yield of ring} - \text{opened hydroxy nitrate } (C_{10}H_{17}NO_4) \text{ at } \tau_{bimolecular} = 0.001 \text{ s}} = 2$$

477   At $\tau_{bimolecular}$ = 10 s, unimolecular reaction dominates the fate of β-pinene ring-opened RO_2, roughly

478   70% of which undergoes endo-cyclization, based on our theoretical calculations (Scheme 2C).

479   This suggests that

480    $$\frac{\text{yield of endoperoxide hydroxy } RO_2 \ (C_{10}H_{17}O_5) \text{ at } \tau_{bimolecular} \ = \ 10 \text{ s}}{\text{yield of ring} - \text{opened } RO_2 \ (C_{10}H_{17}O_3) \text{ at } \tau_{bimolecular} \ = \ 0.001 \text{ s}} = 0.7$$

481   At $\tau_{bimolecular}$ = 10 s, roughly 56% of endoperoxide hydroxy RO_2 reacts with NO, based on MCM

482   simulation. At $\tau_{bimolecular}$ = 0.001 s, nearly 100% of ring-opened RO_2 is expected to react with NO.

483   Therefore,

484    $$\frac{\text{fraction of } C_{10}H_{17}O_5 + \text{NO at } \tau_{bimolecular} \ = \ 10 \text{ s}}{\text{fraction of } C_{10}H_{17}O_3 + \text{NO at } \tau_{bimolecular} \ = \ 0.001 \text{ s}} = 0.56$$

485   Combining the above three ratios, we estimate that

486    $$\frac{BR_{RONO2} \text{ of endoperoxide hydroxy } RO_2 \ (C_{10}H_{17}O_5)}{BR_{RONO2} \text{ hydroxy } RO_2 \ (C_{10}H_{17}O_3)} = \frac{2}{0.7 \times 0.56} = 5.1$$

487   As endoperoxide hydroxy RO_2 and ring-retained hydroxy RO_2 share similar structure (i.e., β-

488   hydroxy RO_2 with two rings), we expect they have similar BR_{RONO2}. Thus, we infer $BR_{RONO2,β\text{-}}$

489    $_{OH,3rd}$/$BR_{RONO2,ring\text{-}open}$ to be 5.1, which is close to the ratio, 4.3, found by solving the system of

490   equations.

491   5) $BR_{acetone}$ represents the branching ratio to form acetone. This branching ratio is calculated

492   to be nearly zero as an earlier theoretical study suggested that the endo-cyclization has an energy

493   barrier about 3.6 kcal mol^{-1} lower than that of acetone elimination[61].

494   6)   The β-hydroxy alkoxy radicals (R2 and R3 in Scheme S 7) can undergo either H-shift or

495   ring-opening. Peeters et al. assumed that 87.5% of the R2 and R3 would undergo ring-opening and

496   subsequently produce pinonaldehyde. Our MC-TST calculations, however, suggest that H-shift of

497   some R2 isomers can be competitive with its ring-opening reaction. F12 level of theory calculates

498   that for the A3 and A9 (in Scheme S 2) derived alkoxy radical, the 1,5 H-shift from the methyl

499   group (i.e., C9 points towards the ring and towards the alkoxy radical) to the alkoxy group proceeds

500   at a rate of 1.9×10^8 s^{-1} (Table S 19). The H-shift channel is estimated to account for 35% of the

501   fate of these alkoxy radicals. We note that the H-shift reaction is possible only for the isomers

502   which have the alkoxy radical on the same side of the ring as the two methyl groups on the four-

503   membered ring (i.e., A3, A5, A7, and A9 derived alkoxy radical). The H-shift from CH_2 group to

504   alkoxy radical may also be important, but not examined yet. Therefore, the branching ratios of R2

505   and R3 warrant future investigation.

506   7)   The α-hydroxyalkylperoxy radical (R5 and R6 in Scheme S7) can undergo either thermal

507   decomposition to produce pinonaldehyde or reaction with NO. Peeters et al. estimated thermal

508   decomposition rate to be ~ 2000 s^{-1} at room temperature, making this reaction the dominant fate

509   of α-hydroxyalkylperoxy in the atmosphere. However, Peeters et al. argued that in some laboratory

510   studies where NO concentrations are of the order of 10-100 ppm, a significant fraction of α-

511   hydroxyalkylperoxy would react with NO and lower the pinonaldehyde yield. The calculated

512   pinonaldehyde yield is 35.7% under "laboratory conditions" (where 60% of α-hydroxyalkylperoxy

513   undergoes thermal decomposition) and 59.5% under "ambient conditions" (where 100% of α-

514   hydroxyalkylperoxy undergoes thermal decomposition). However, many laboratory studies have

515   been performed under conditions close to "ambient conditions" and yet report much lower

516   pinonaldehyde yields than the calculation. For example, Aschmann et al. quantified pinonaldehyde

517   yield where initial NO concentration was 200 ppbv[62]. Using 9.15×10^{-12} s^{-1} as the RO$_2$+NO reaction

518   rate coefficient (from MCM), roughly 98% of α-hydroxyalkylperoxy in the Aschmann et al. study

519   undergoes thermal decomposition, a condition similar to "ambient condition" reported in Peeters

520   et al. However, the measured yield is 28±5%, roughly a factor of two lower than that calculated in

521   Peeters et al. Similarly, Wisthaler et al. measured the pinonaldehyde yield to be 34±9% when

522   initial NO is in the range of 1-2ppm (i.e., ~90% of α-hydroxyalkylperoxy undergoes thermal

523   decomposition)[63]. Therefore, the pinionaldehyde yield calculated in Peeters et al. is likely over-
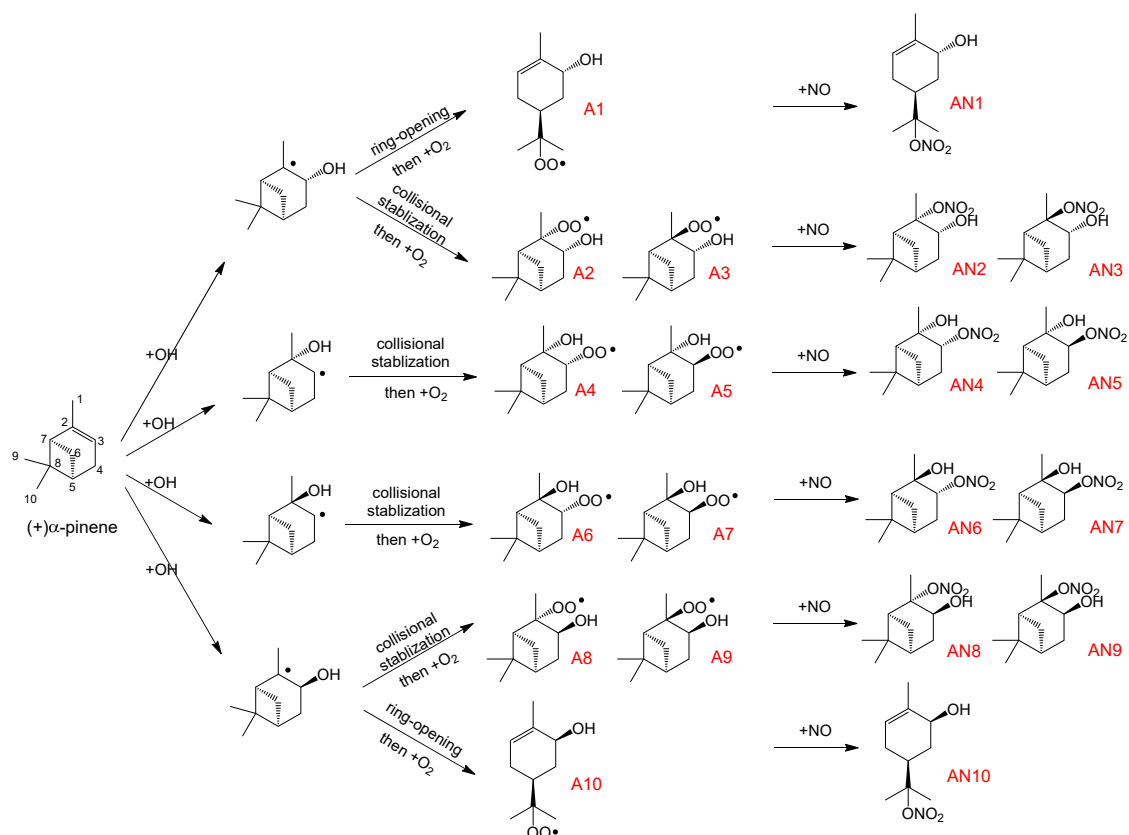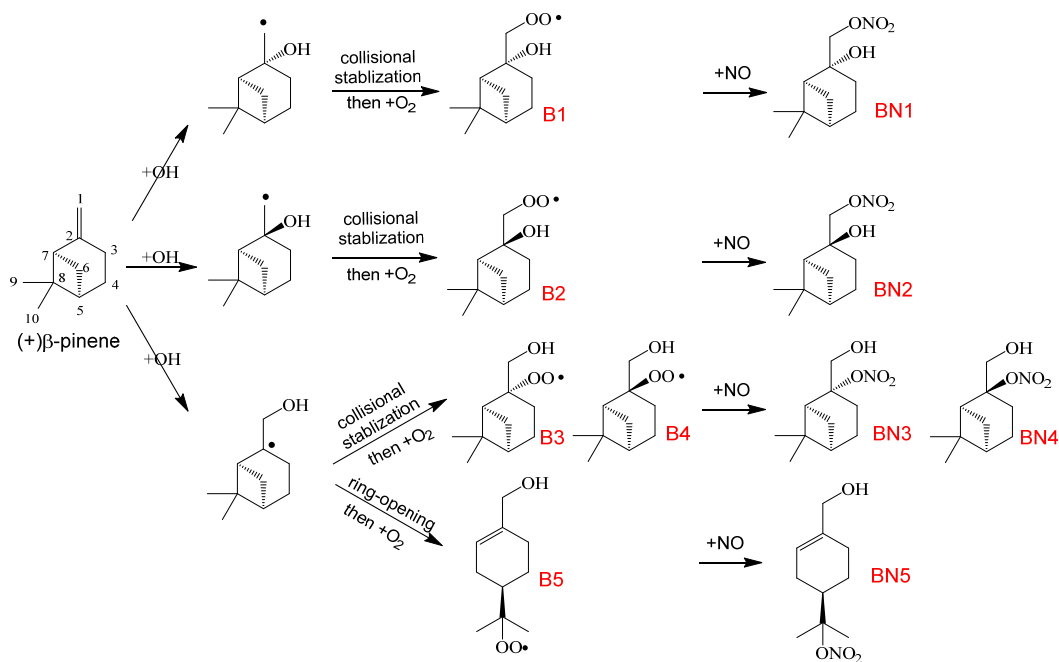
524   estimated.

525

526
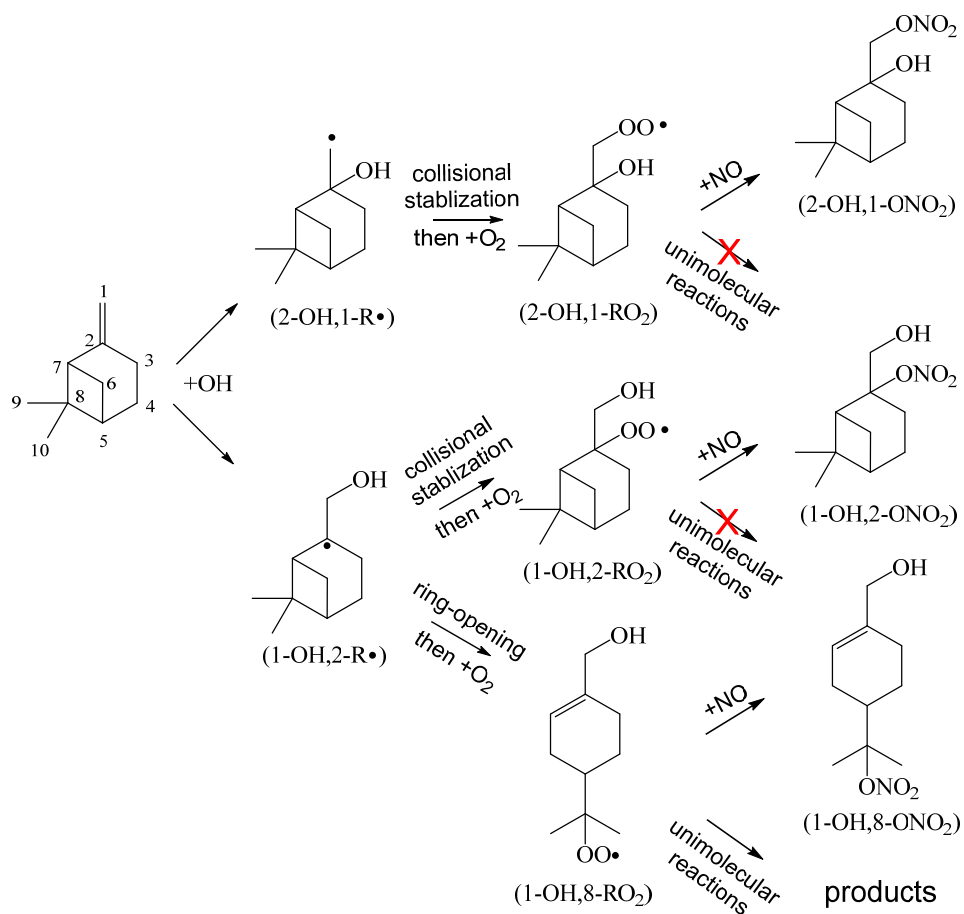
Scheme S 1. The simplified oxidation mechanism of β-pinene + OH. Each structural isomer of RO$_2$ and hydroxy nitrate has multiple diastereoisomers, which are shown in Scheme S 2. The RO+NO$_2$ produced from RO$_2$+NO reactions are not included in the scheme for clarity.
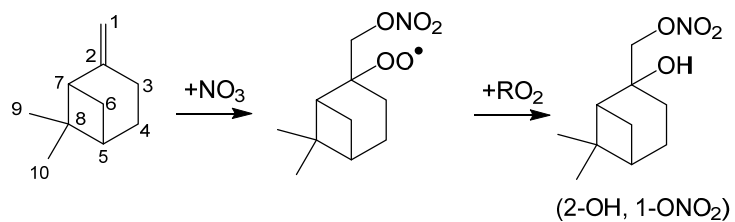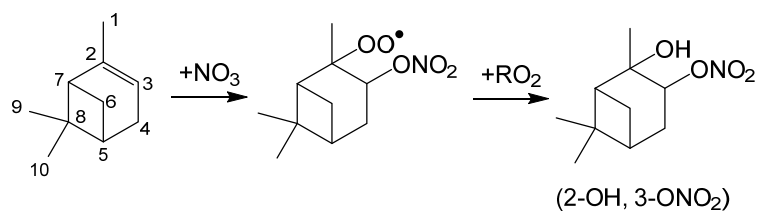
530

531

Scheme S 2. The formation of (a) ten isomers of (+) α-pinene hydroxyl nitrates (AN1-AN10) and (b) five isomers of (+) β-pinene hydroxyl nitrates (BN1-BN5). (-) β-pinene is used in experiments, but (+) β-pinene is used in computational calculations. The RO+NO_2 produced from RO_2+NO reactions are not included in the scheme.

536

537 Scheme S 3. The reaction of α-pinene and β-pinene with NO_3 radical and subsequently with
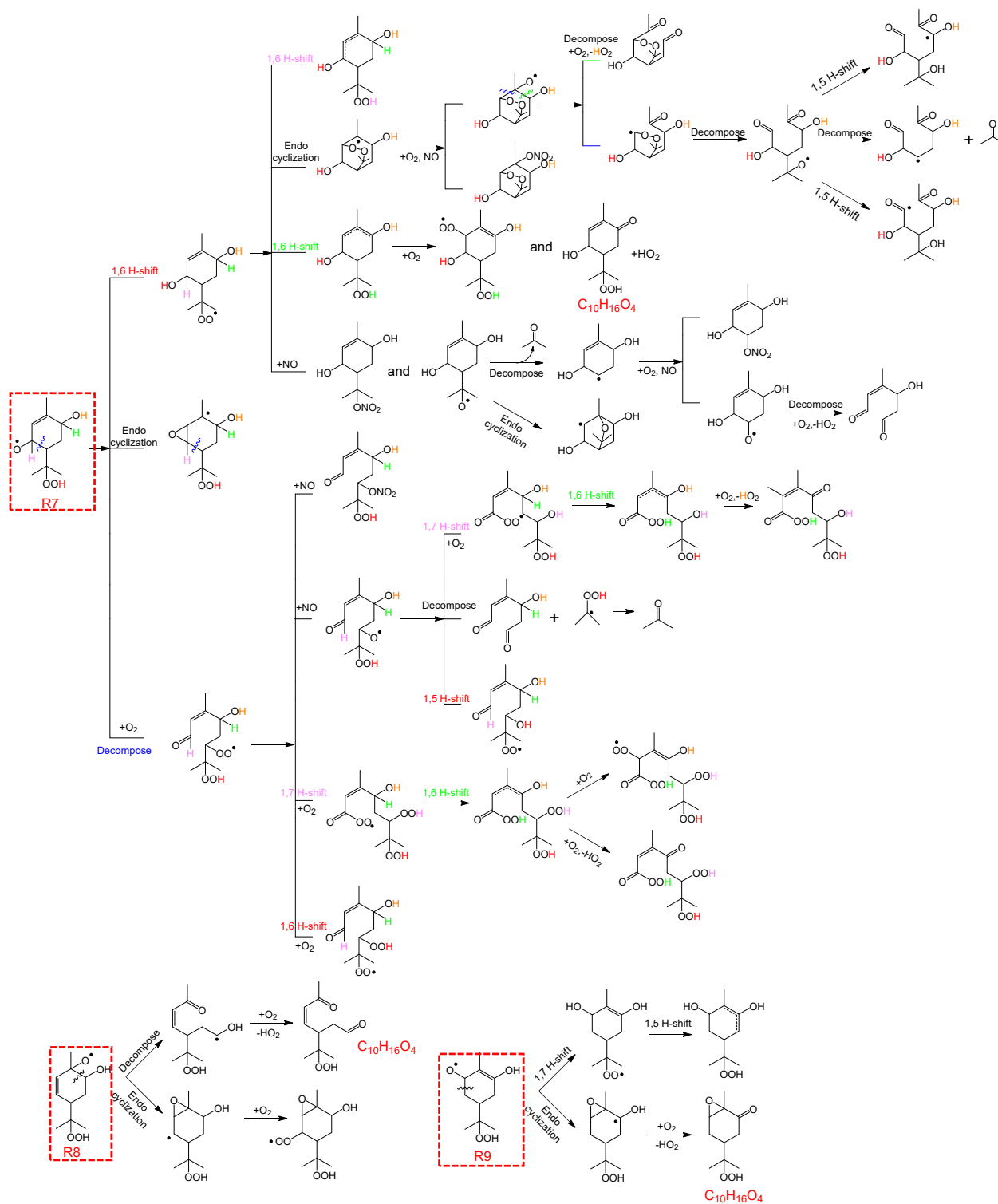538 another RO_2.

539

540
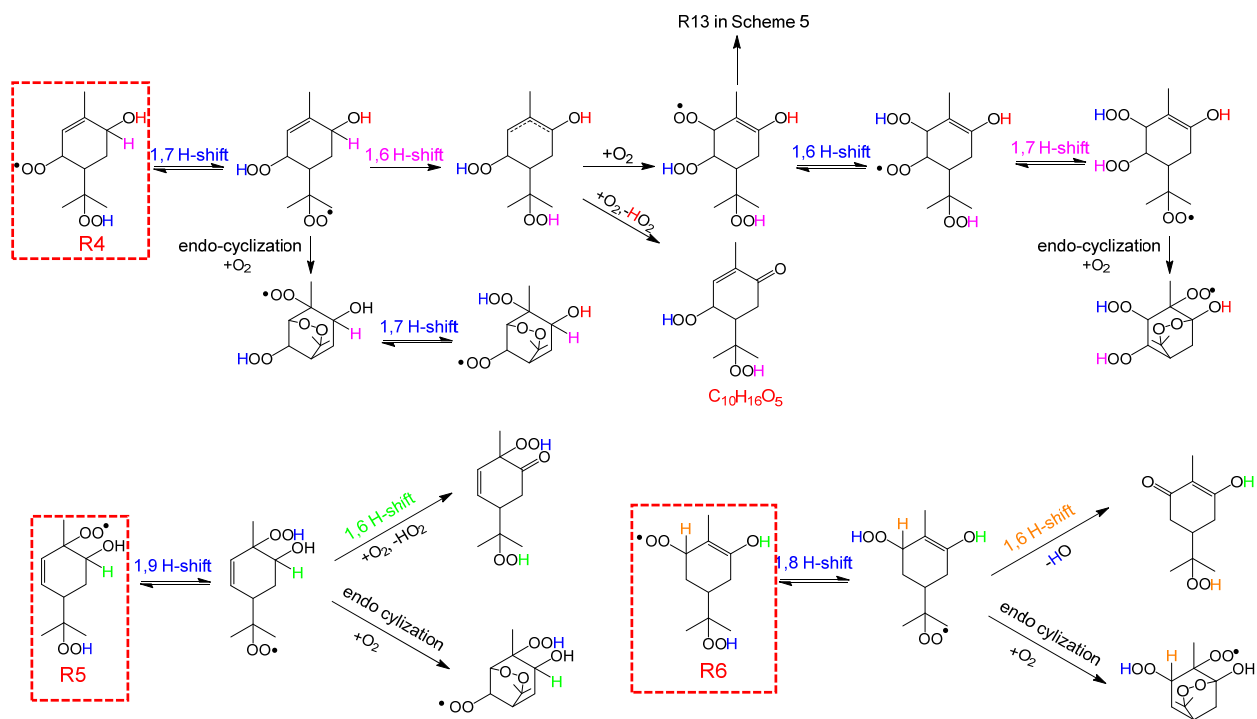
Scheme S 4. Speculations on the potential reactions of three α-pinene second-generation RO_2 (shown in red boxes). There are a number of potential reactions pathways not included in the scheme.
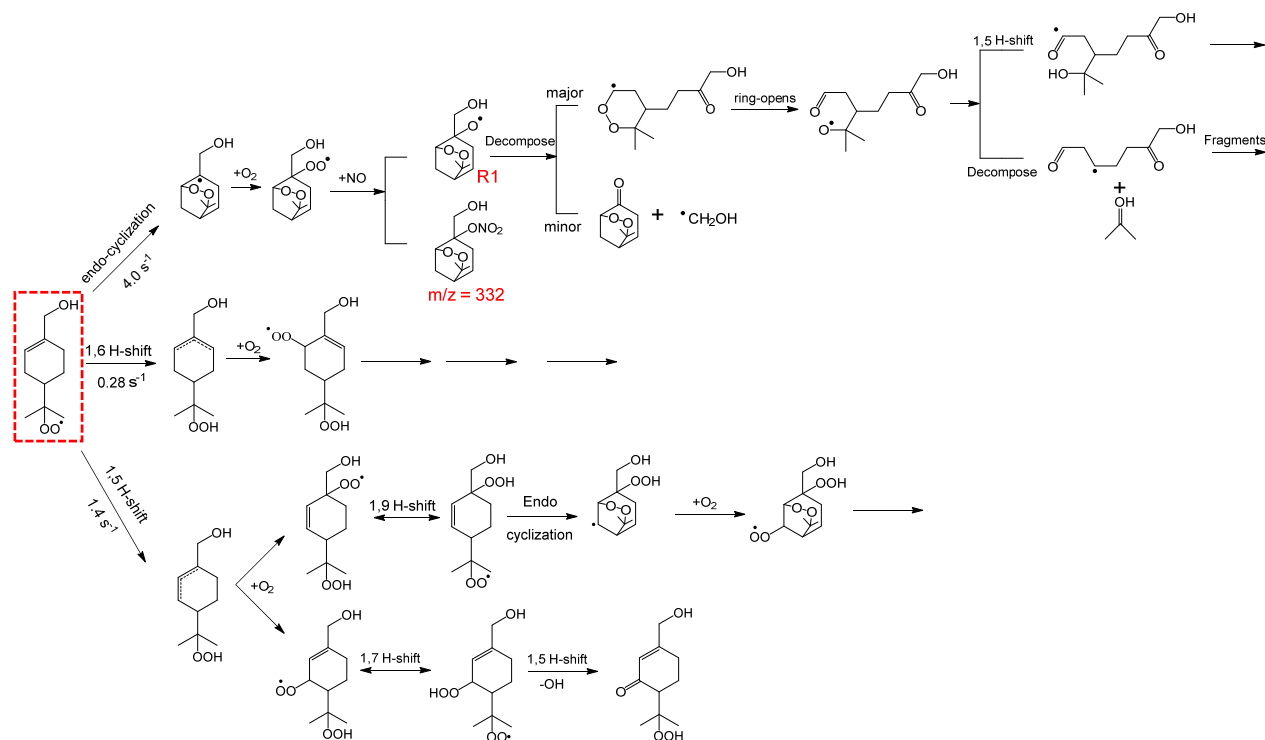
545

Scheme S 5. Speculations on the reactions of α-pinene second-generation alkoxy radicals (shown
in red boxes). There are a number of potential reactions pathways not included in the scheme.

548

549

550   Scheme S 6. Speculations on the reactions of β-pinene 1-OH,8-RO$_2$ (shown in red box) following
551   the dominant initial unimolecular reactions. Rate coefficients for these are calculated using the
552   approach by Møller et al. [24]. There are a number of potential reactions pathways not included in
553   the scheme. ωB97X-D/aug-cc-pVTZ barrier heights suggest suggest that the major decomposition
554   pathway of R1 in this scheme is towards the –OO group (Table S 14).
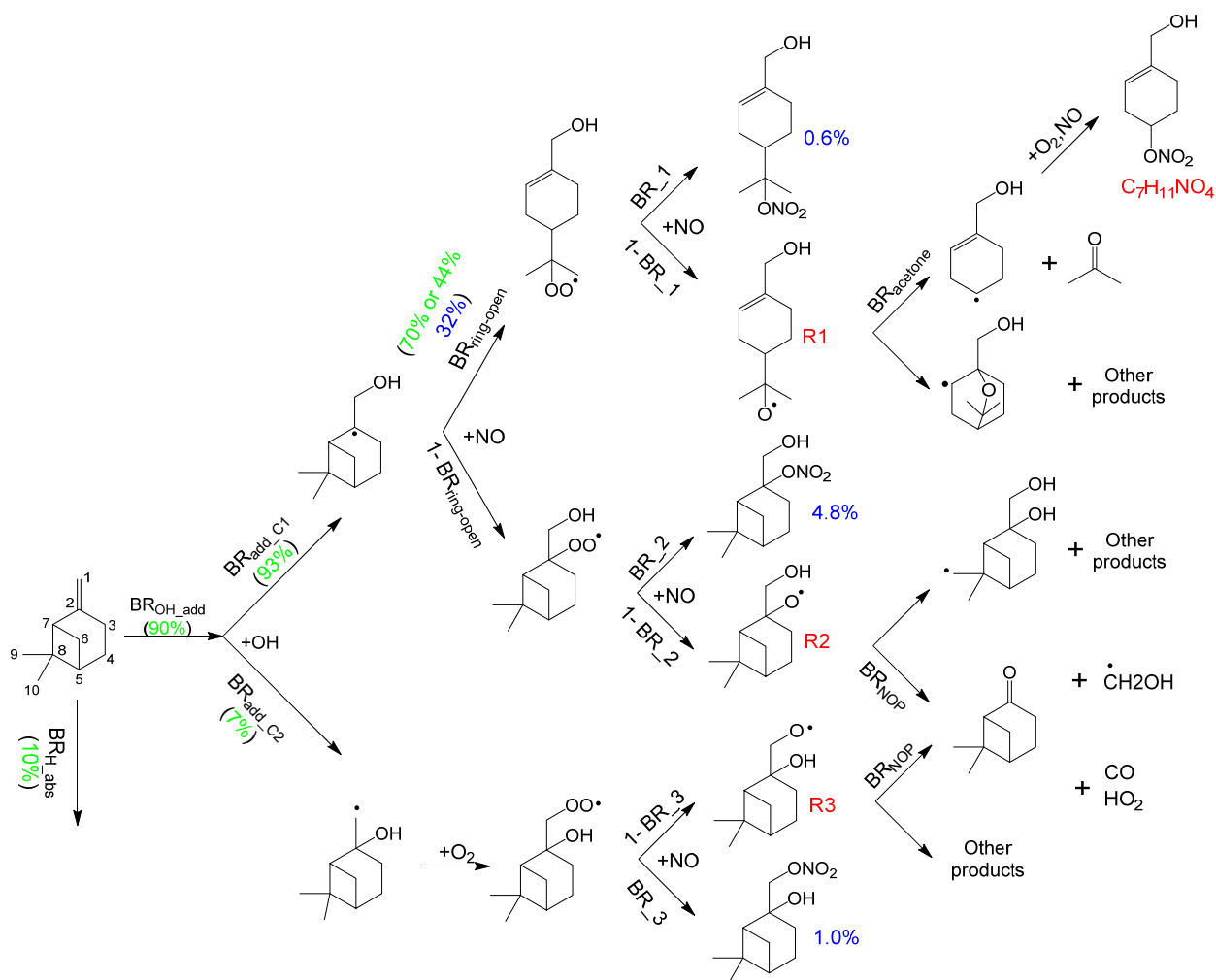
555

556
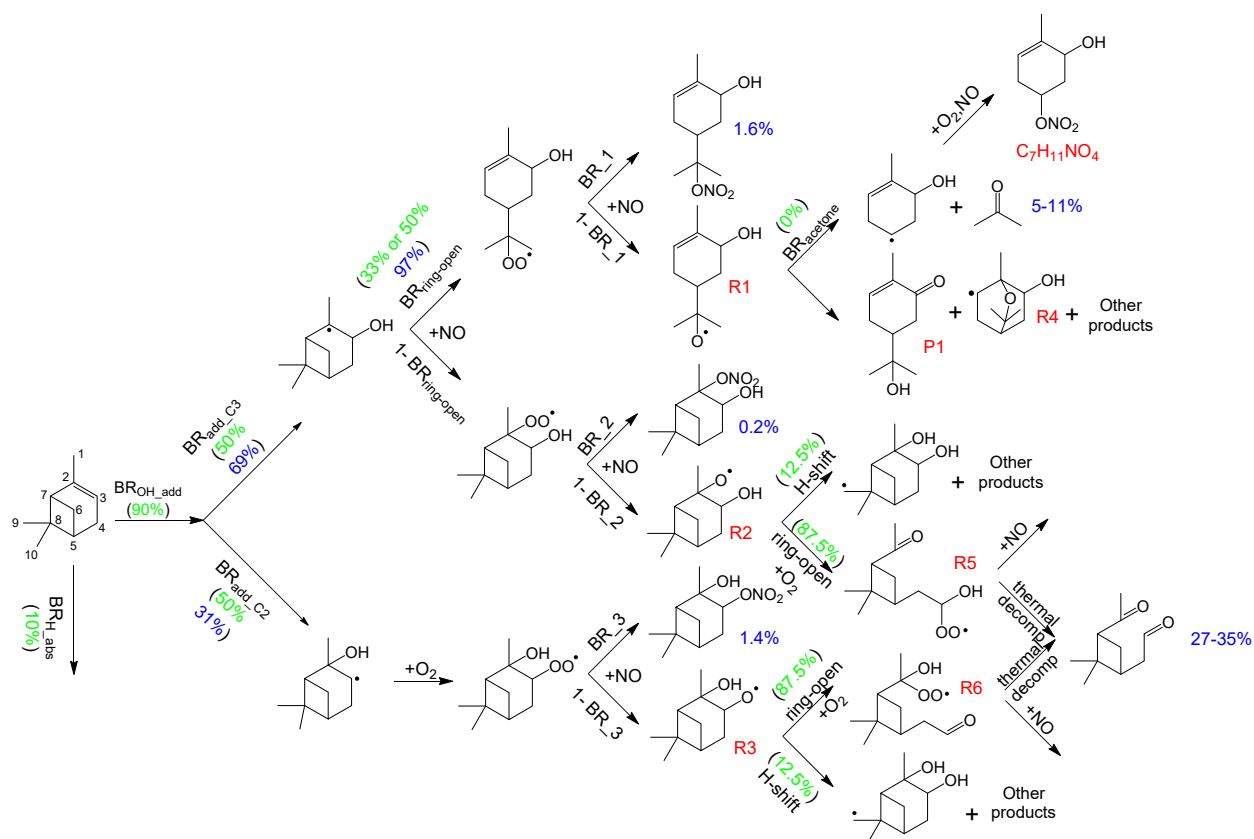
Scheme S 7. The simplified formation mechanism of hydroxy nitrates and co-products for α-pinene. The numbers marked green are from computational calculations. The numbers marked blue are experimentally constrained in this study or in the literature. The NO_2 produced from RO_2+NO is not shown in the scheme. The branching ratios of the following steps are discussed in the section S6. (1) BR_{H_abs} and BR_{OH_add} refer to the branching ratios of α-pinene reaction with OH via H abstraction and OH addition, respectively. (2) BR_{add_C2} and BR_{add_C3} refer to the branching ratios that OH addition to C2 and C3, respectively. (3) $BR_{ring-open}$ refers to the ring-opening fraction of alkyl radical. (4) "BR" refers to the nitrate branching ratio. (5) $BR_{acetone}$ refers to the branching ratio to form acetone. (6) "H-shift" and "ring-open" refer to the H-shift and ring-opening of R2 and R3. (7) "thermal decomp" and "+NO" refer to thermal decomposition and reaction with NO for R5 and R6.

568

S28

569

Scheme S 8. The simplified formation mechanism of hydroxy nitrates and co-products for β-pinene. The numbers marked green are from computational calculations. The numbers marked blue are experimentally constrained in this study or in the literature. The NO_2 produced from RO_2+NO is not shown in the scheme. BR_{H_abs} and BR_{OH_add} refer to the branching ratios of β-pinene reaction with OH via H abstraction and OH addition, respectively. BR_{add_C1} and BR_{add_C2} refer to the branching ratios that OH addition to C1 and C2, respectively. $BR_{ring-open}$ refers to the ring-opening fraction of alkyl radical. "BR" refers to the nitrate branching ratio (Table S 21). $BR_{acetone}$ refers to the branching ratio to form acetone. BR_{NOP} refers to the branching ratio to form nopinone.
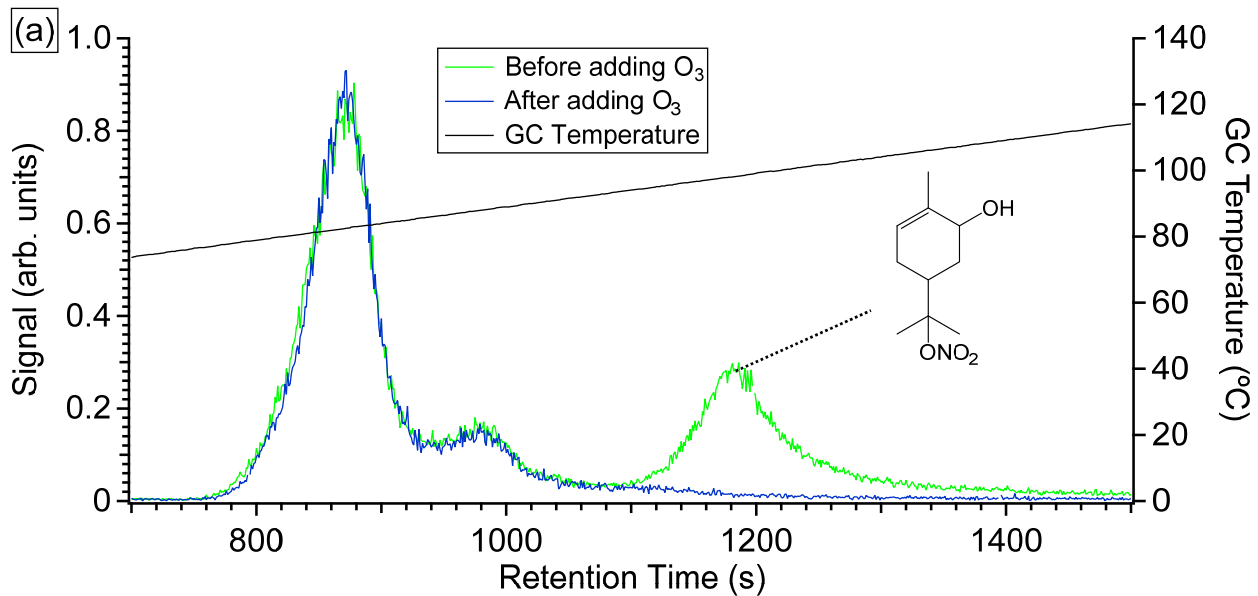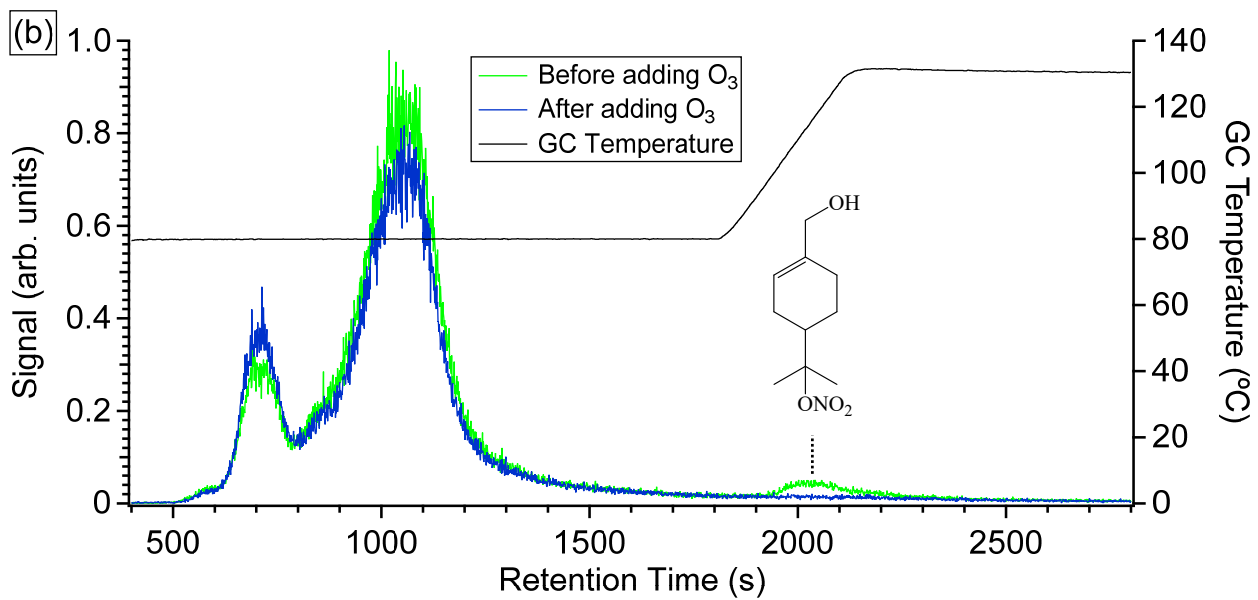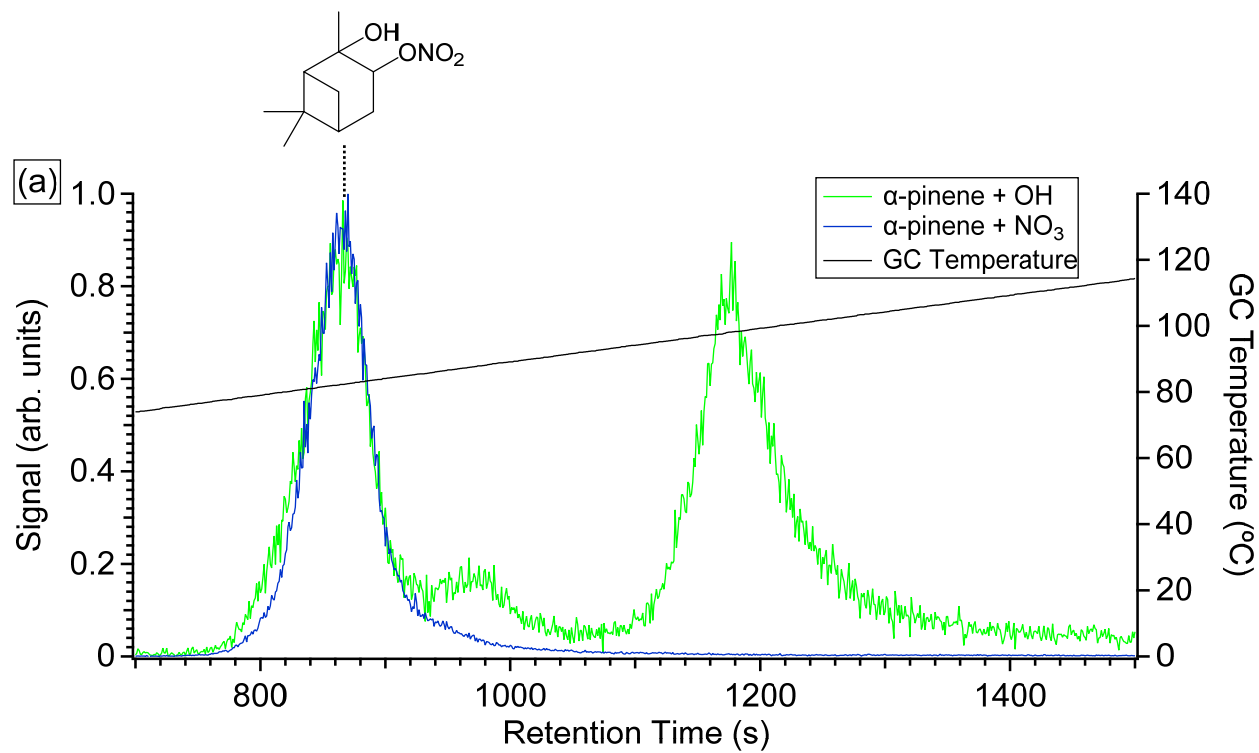
Figure S 1. The effects of adding O₃ on the distribution of (a) α-pinene and (b) β-pinene hydroxy nitrates. The black lines are the GC temperature.

583

584

585
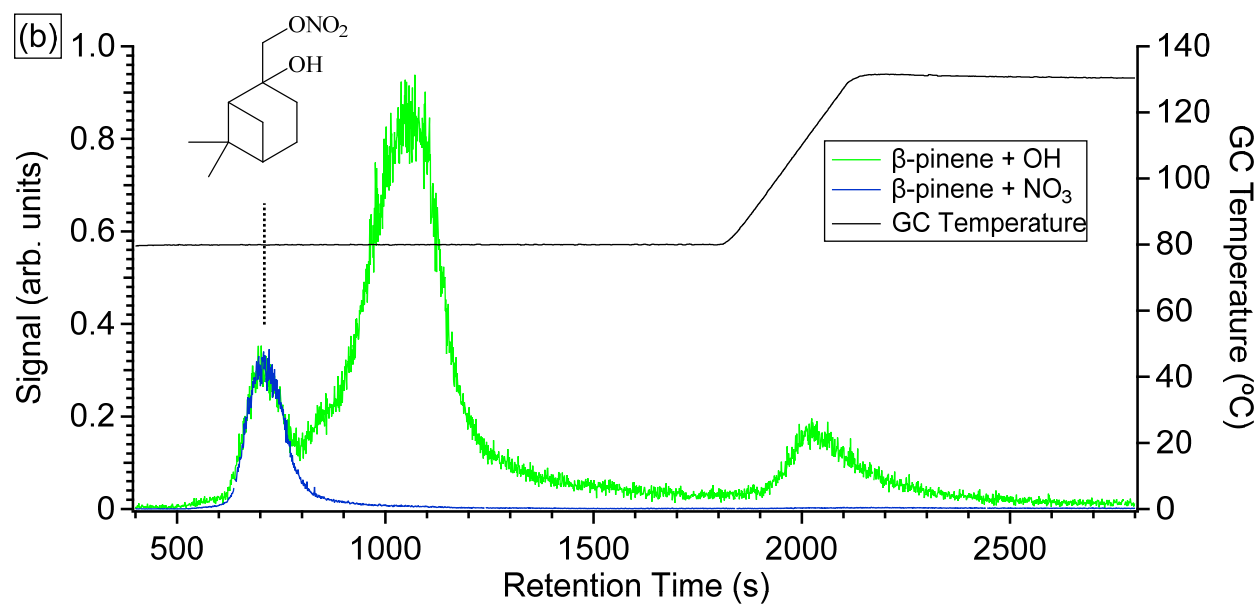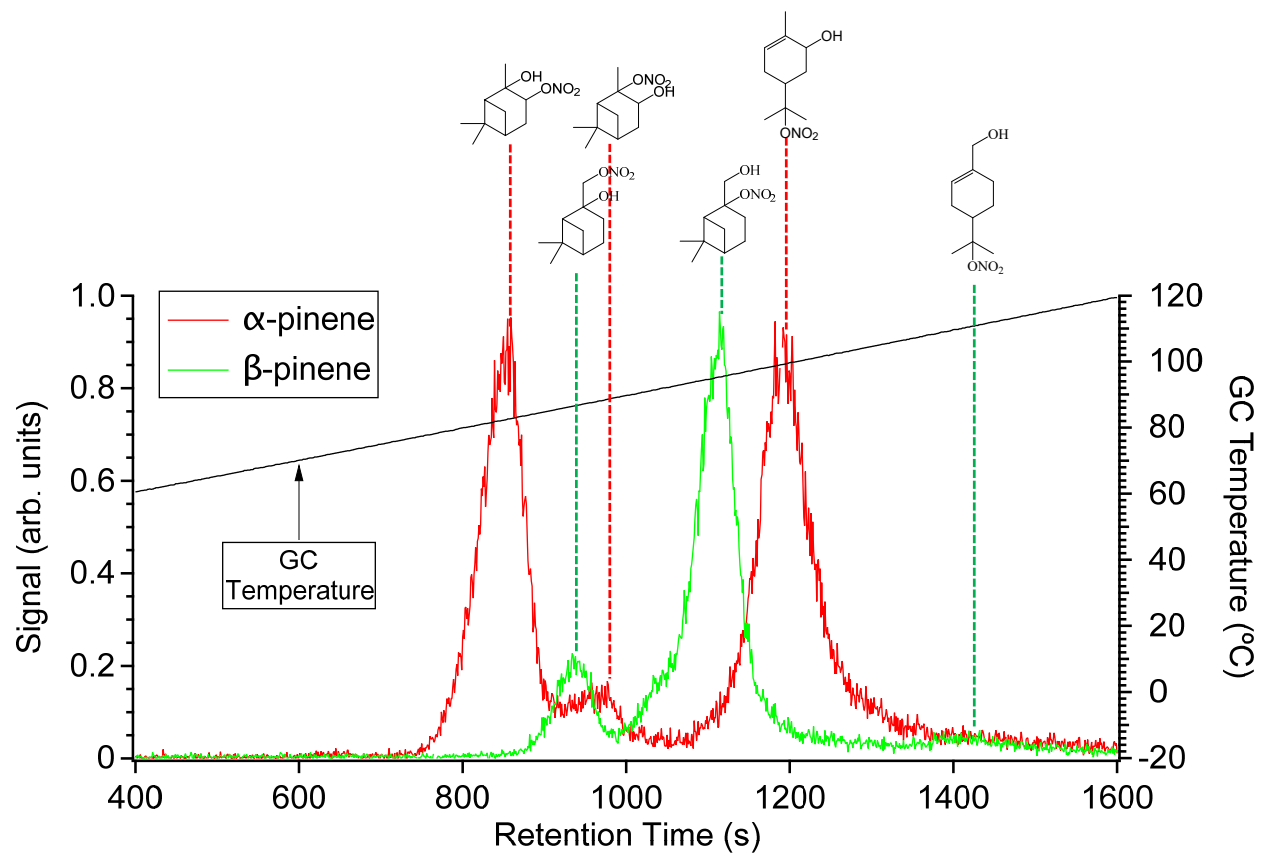
586

587

588   Figure S 2. The distributions of (a) α-pinene and (b) β-pinene hydroxy nitrates from OH oxidation
589   and NO$_3$ oxidation. The black lines indicate the GC temperature.

590

591

592

593

Figure S 3. The comparison between the distributions of α-pinene and β-pinene hydroxyl nitrates
using the same temperature profile. The black lines indicate the GC temperature.

596

597

598
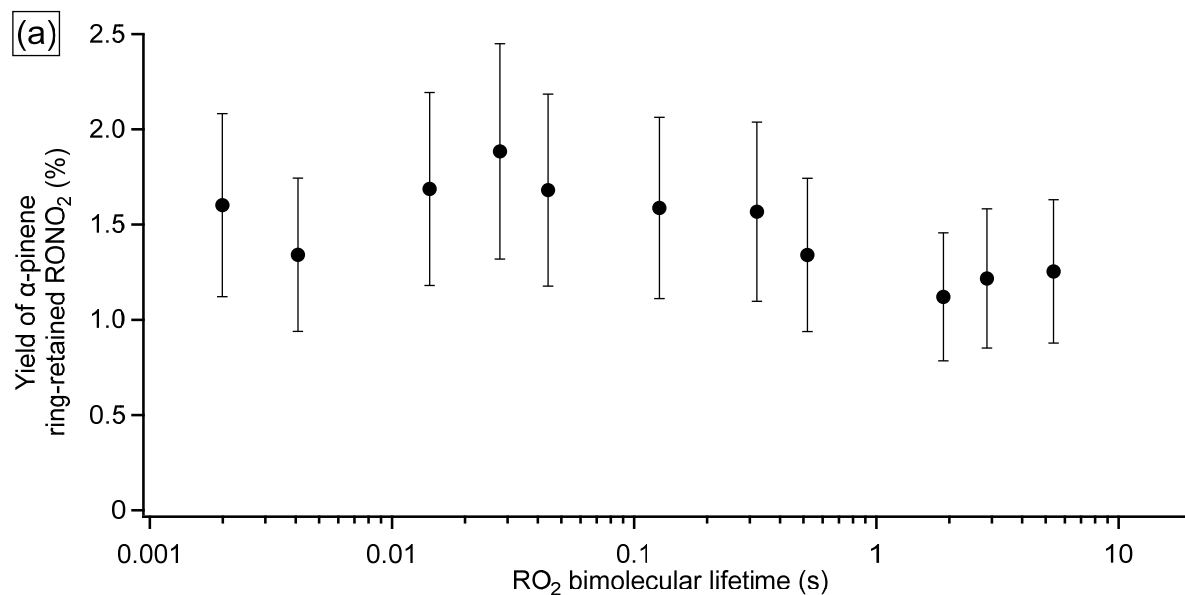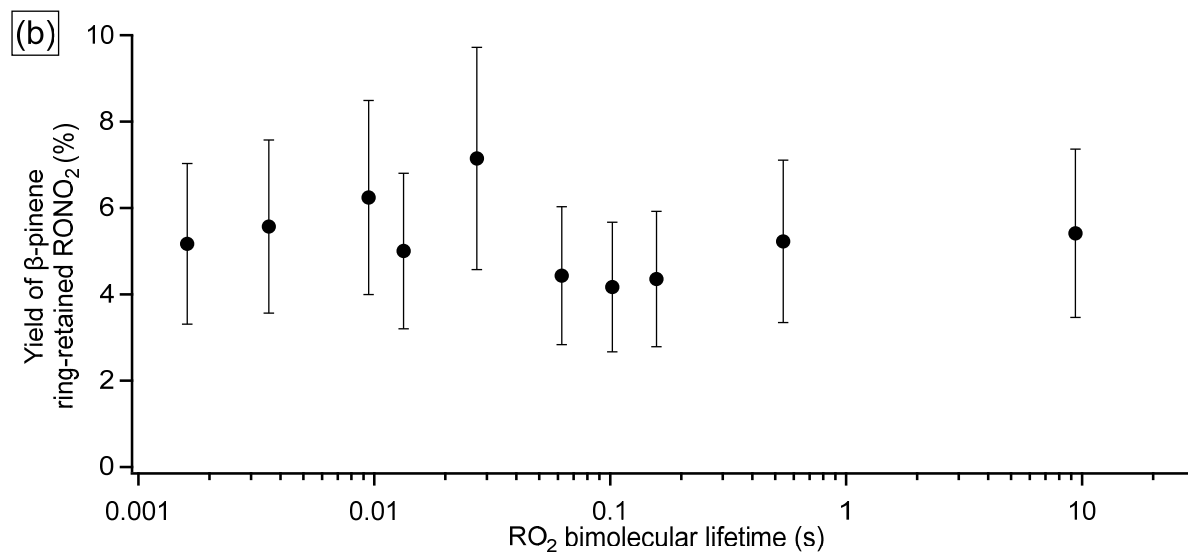
Figure S 4. The summed yield of two structural isomers of ring-retained hydroxy nitrates of (a) α-pinene and (b) β-pinene as a function of RO_2 bimolecular lifetime. The ratio between two structural isomers of ring-retained HNs (e.g., α-pinene 2-OH,3-ONO_2/3-OH,2-ONO_2) does not change with $\tau_{bimolecular}$ (shown in Figure 1). For experiments with $\tau_{bimolecular}$ longer than 1 s, the yield is corrected by the fraction of RO_2 that reacts with NO, which is estimated from MCM as described in Section S2.

605
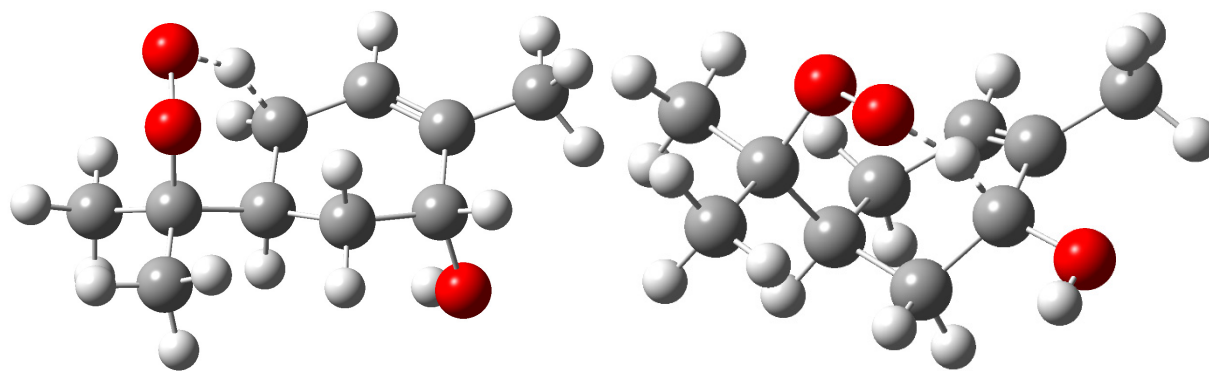
Figure S 5. Lowest-energy TS conformer for the 1,5 (left) and 1,6 (right) H-shift forming an allyl radical in the ring-opened *anti* α-pinene peroxy radical (α-pinene *anti* 3-OH,8-RO$_2$). The structures are optimized at the ωB97X-D/aug-cc-pVTZ level of theory. The same is observed in the *syn* α-pinene 3-OH,8RO$_2$ and β-pinene 1-OH,8-RO$_2$ systems.

610

611   (a) α-pinene   (b) α-pinene   (c) β-pinene

612   *anti* 3-OH,8-RO$_2$ *syn* 3-OH,8-RO$_2$ 1-OH,8-RO$_2$

613

614   Figure S 6. The lowest-energy conformers of the TS for formation of the 6-membered
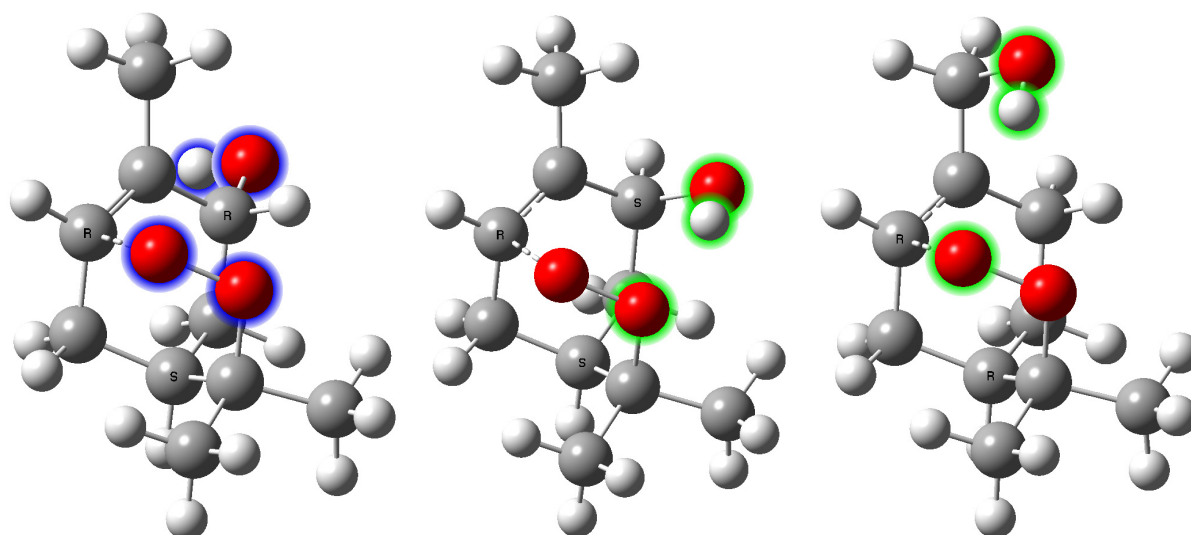615   endoperoxide in (a) α-pinene *anti* 3-OH,8-RO$_2$; (b) α-pinene *syn* 3-OH,8-RO$_2$ and (c) β-pinene 1-
616   OH,8-RO$_2$. Green halos indicate that atoms are involved in the hydrogen bond-like interaction.
617   Blue halos are used when no such interaction exists. We calculated (F12 electronic energy with
618   ωB97X-D/aug-cc-pVTZ zero-point energy correction) that the barrier for ring closure is 2.5
619   kcal/mol larger for α-pinene *anti* 3-OH,8-RO$_2$ than *syn* conformer. The different H-bonding for α-
620   pinene *anti* vs. *syn* 3-OH,8-RO$_2$ has previously been proposed by Vereecken et al. [61], with a
621   calculated barrier difference (B3LYP) of ~2 kcal/mol between *anti* and *syn*.

622

623
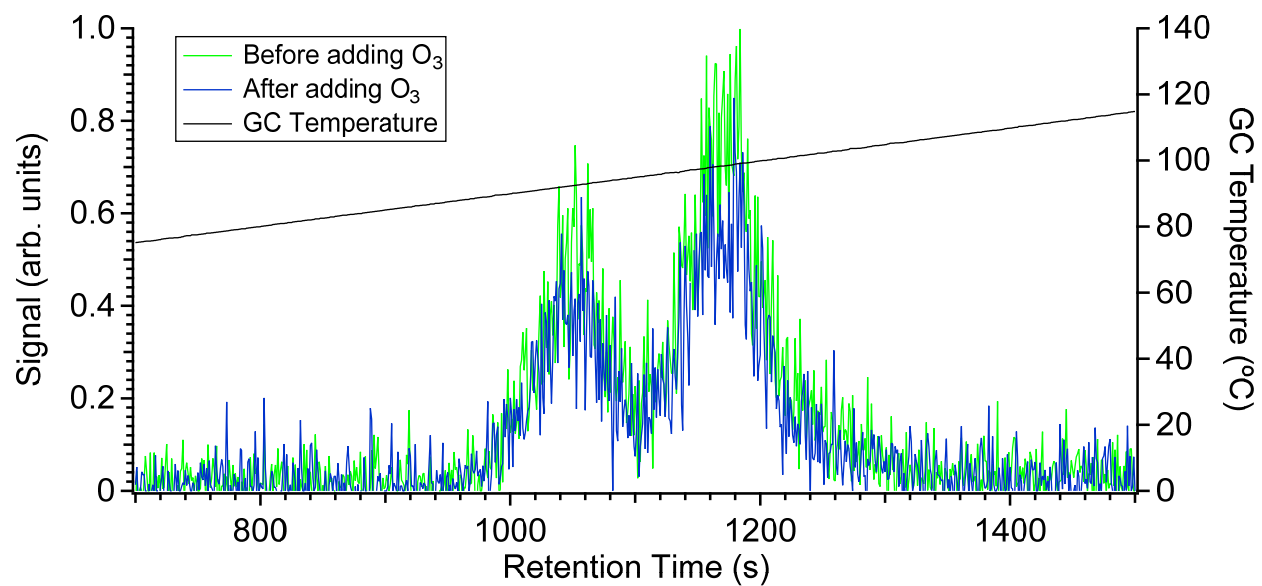
Figure S 7. The effects of adding O_3 on the *m/z* 332 from the α-pinene photooxidation. The black lines are the GC temperature. Note the GC column flow is 7 sccm in this experiment, instead of 5 sccm in other experiments. 2.5 ppmv O_3 is added to the chamber after the photooxidation. GC is taken 1 hr after adding O_3.

628
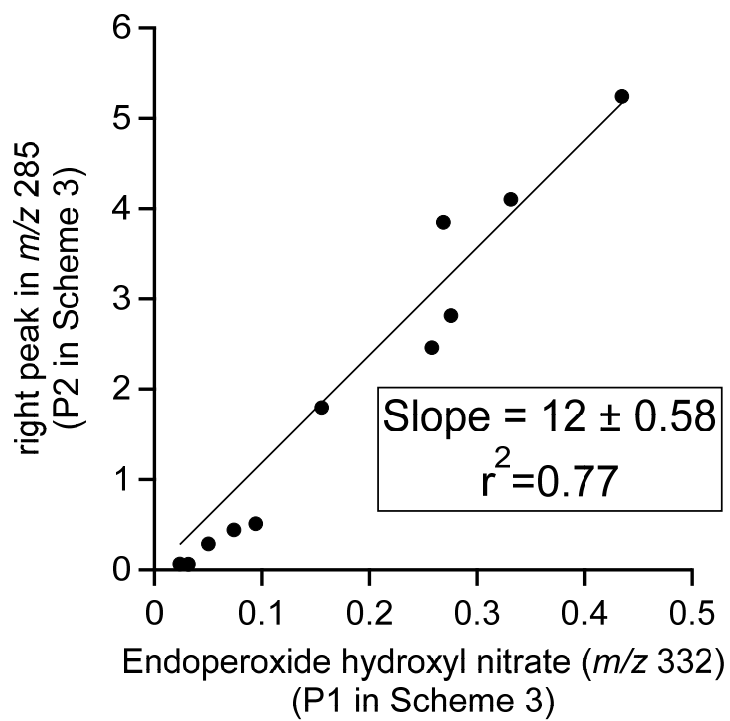
Figure S 8. The correlation between the abundances of the right peak at *m/z* 285 (in Figure 3) and endoperoxide hydroxyl nitrate (*m/z* 332) in α-pinene oxidation. The signals are normalized by the abundance of ring-retained HNs.

629

630
631
632

633

634

635
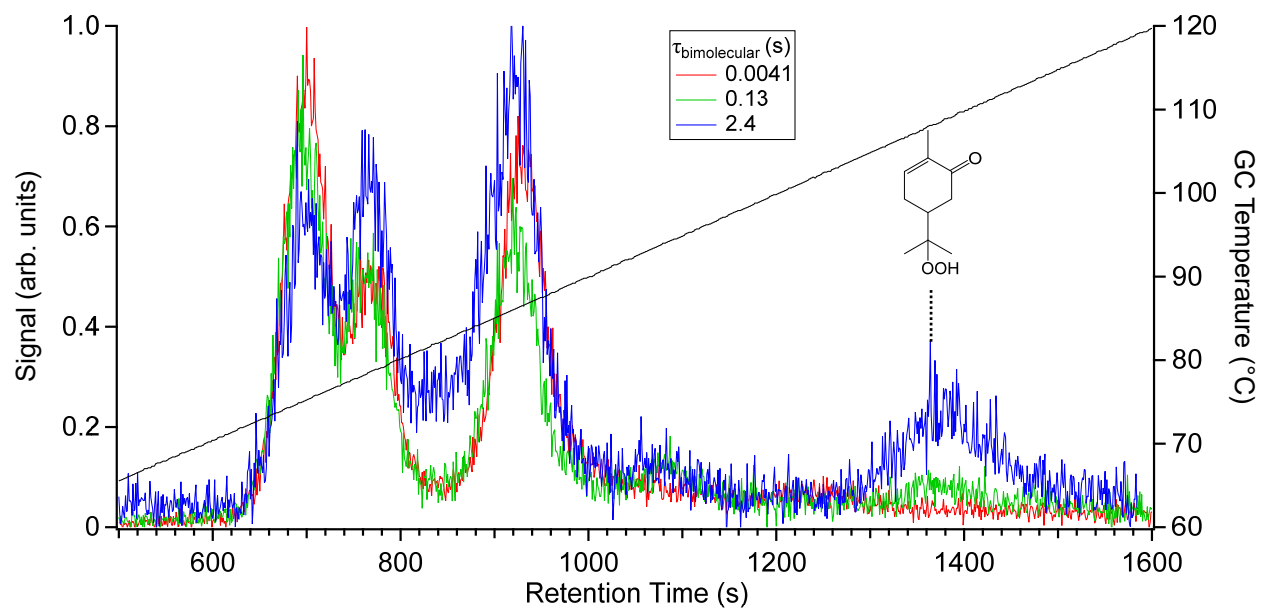
Figure S 9. GC chromatogram of *m/z* 269 in three α-pinene photooxidation experiments with different RO_2 bimolecular lifetime. The signal is normalized by that of ring-retained HNs. The last peak in the chromatogram is tentatively assigned to peroxide ketone (P7 in Scheme 3), mainly because its signal increases with RO_2 bimolecular lifetime.

641

642

643

644

645

646
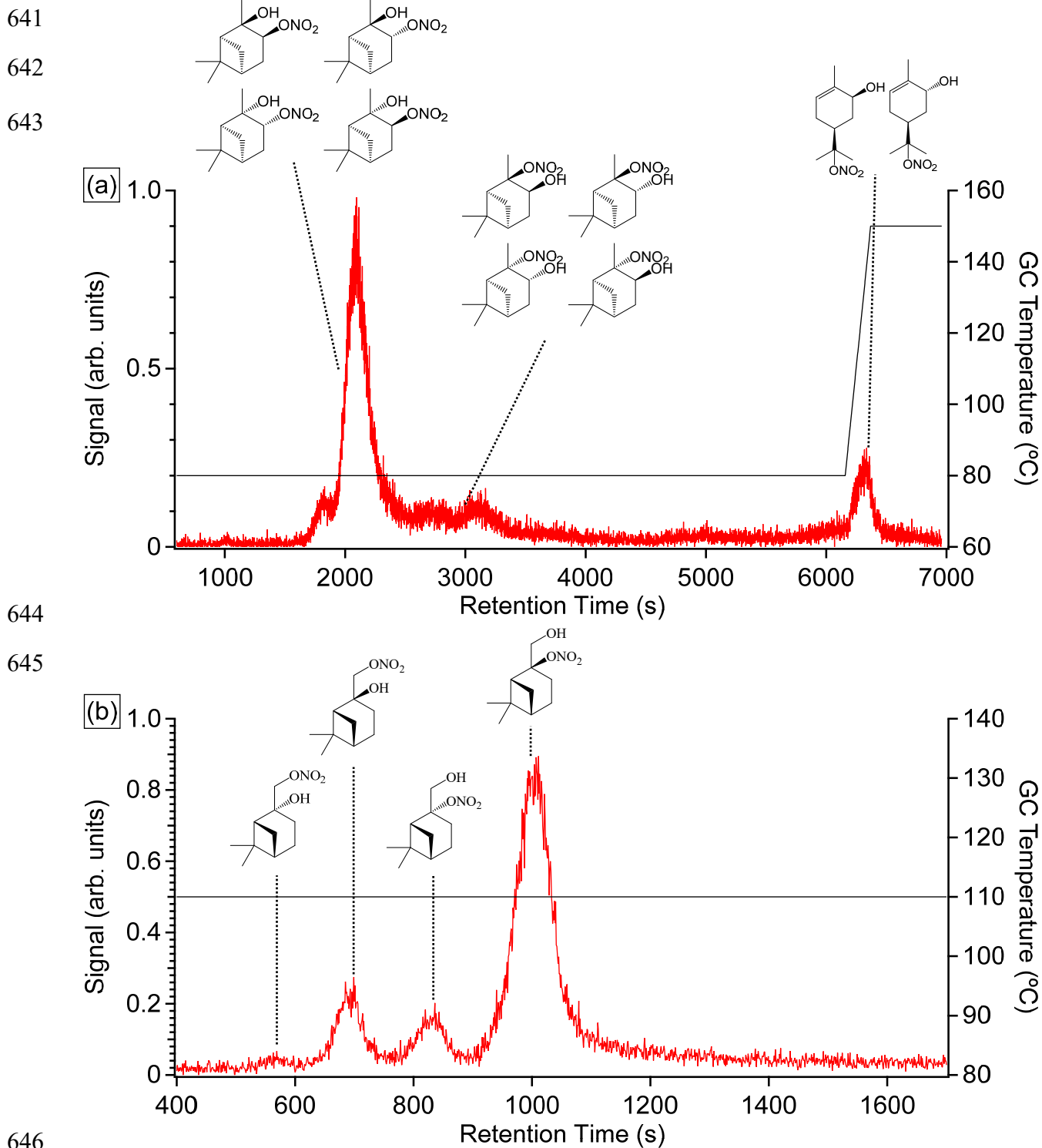
Figure S 10. The distributions of (a) α-pinene and (b) β-pinene hydroxyl nitrates using 5 m GC column. The black lines indicate the GC temperature. α-pinene hydroxy nitrate diastereomers still do not appear to be separated using the 5 m GC. Assignment of the ring-retained isomers is speculative.
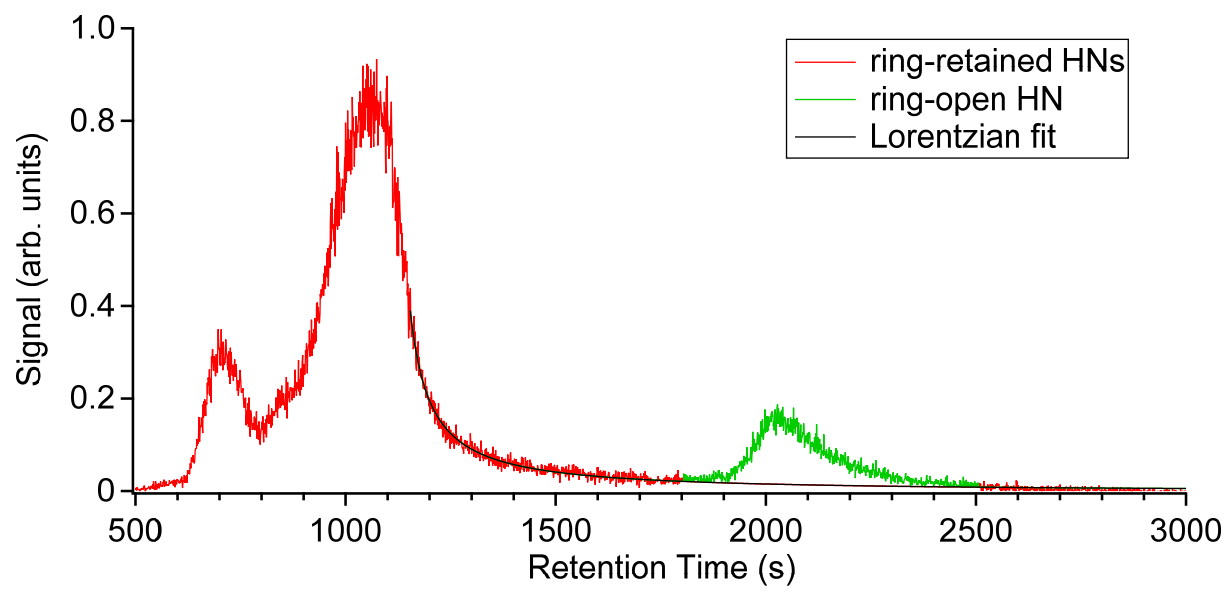
651

652   Figure S 11. The deconvolution of β-pinene hydroxy nitrates.

653

654
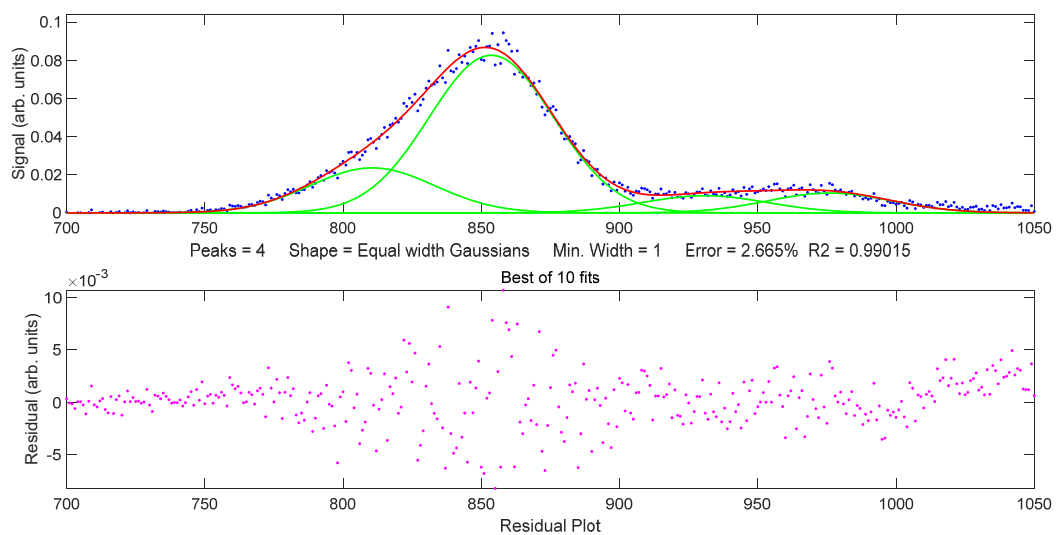
Figure S 12. The peak deconvolution using using four equal-width Gaussian functions[3] for a representative α-pinene hydroxy nitrate distribution. Only the window for ring-retained HNs is shown and fitted.

658

659
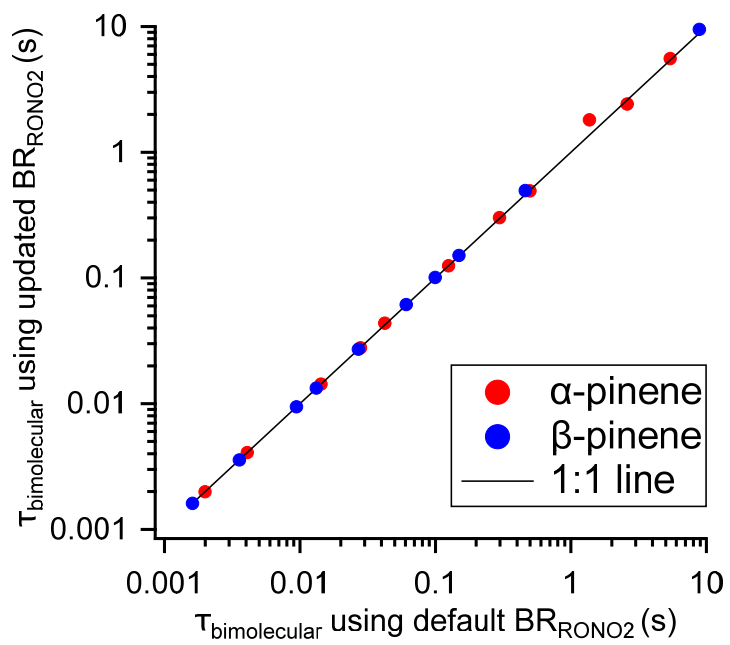
Figure S 13. $\tau_{\text{bimolecular}}$ calculated from MCM by using updated and default nitrate branching ratio.

661
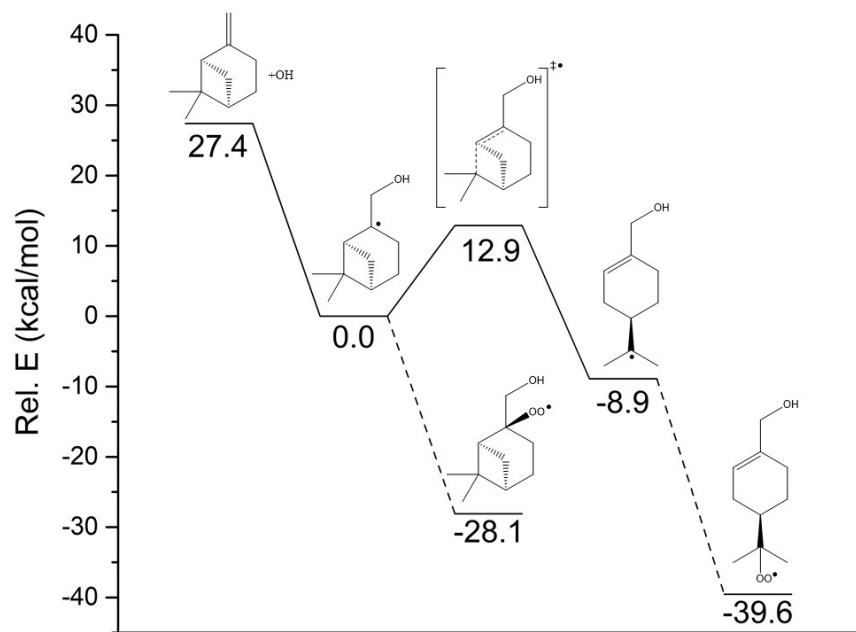
Figure S 14. System modelled for β-pinene with structures of the various compounds.

665

666
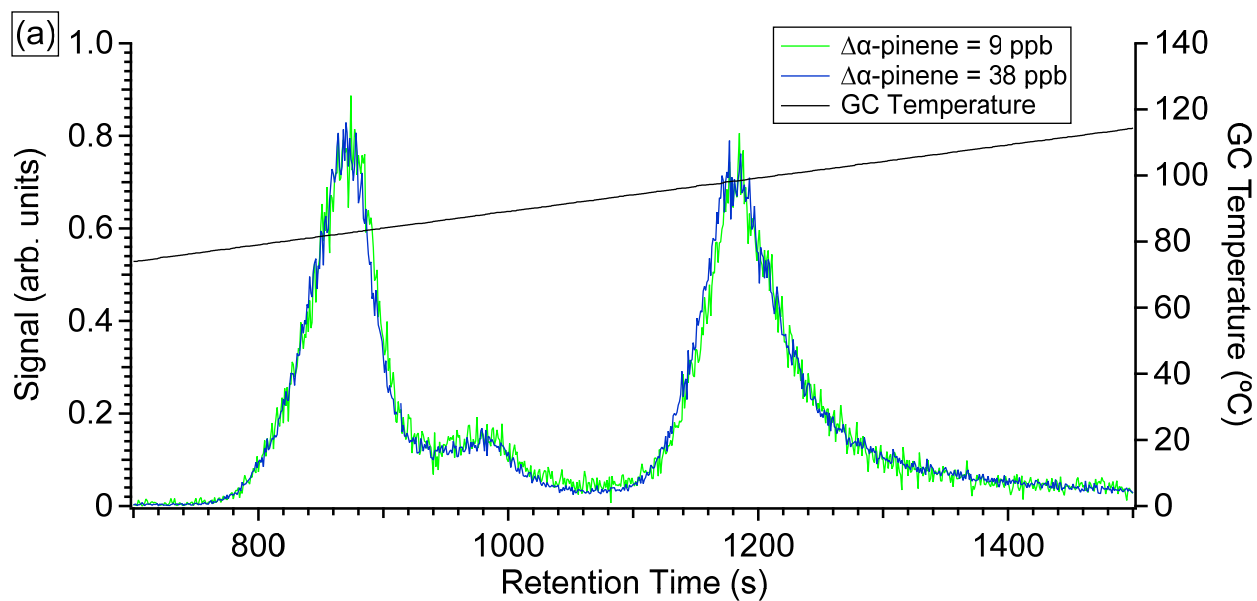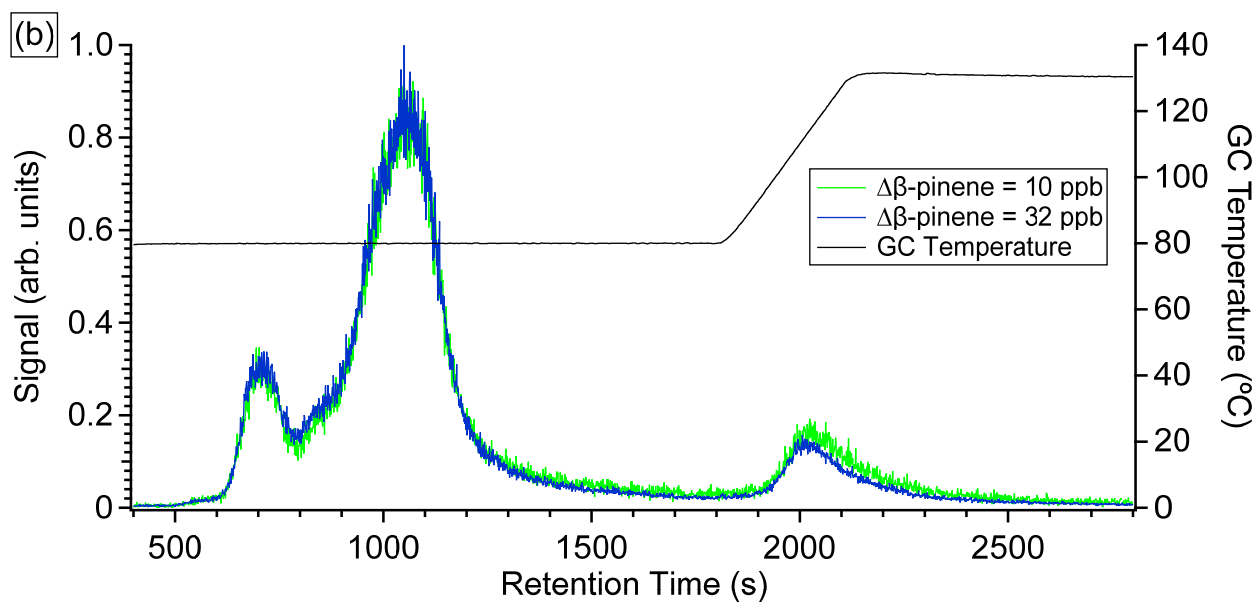
Figure S 15. The effects of gas/particle partitioning on the distribution of (a) α-pinene and (b) β-pinene hydroxyl nitrates. The data are scaled to match the abundance of ring-retained hydroxy nitrates. The black lines indicate the GC temperature.
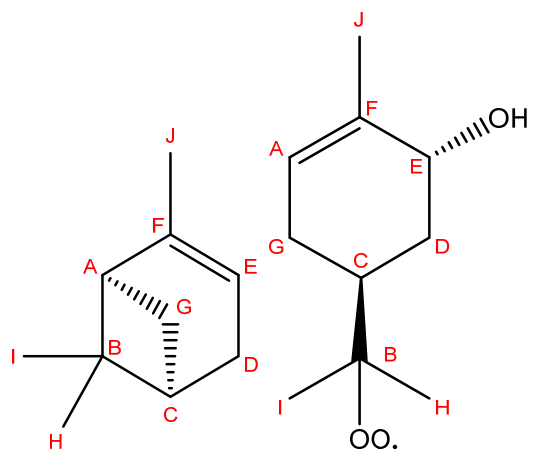
670

671   Figure S 16. Structures of α-pinene (left) and the ring-opened α-pinene peroxy radical (right) with
672   atom labeling of the carbon atoms used to define the unimolecular reactions.

673

674
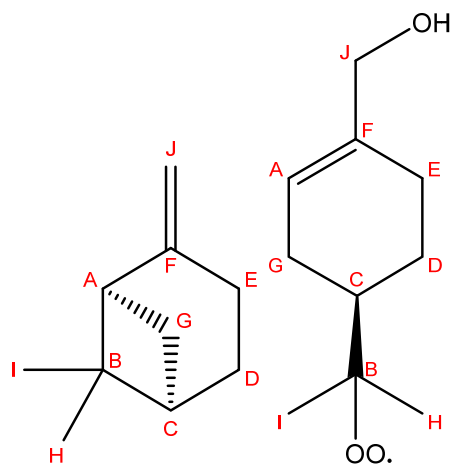
Figure S 17. Structures of β-pinene (left) and the ring-opened β-pinene peroxy radical (right) with atom labeling of the carbon atoms used to define the unimolecular reactions.

677

678   Table S 1. Experimental Conditions.

VOC	Expt No.	Initial Concentration (ppbv)				Oxidation Time (min)	Reacted VOC Conc. (ppbv)	OH exposure (10^9 molec×cm^{-3}×s)
		VOC	CH$_3$ONO	NO	NO$_2$			
α-pinene	1	73.6	68.9	42.6	0.0	3.0	6.3	1.7
	2	108.0	60.2	19.8	0.0	2.5	4.7	0.8
	3	66.2	69.2	15.2	7.4	2.6	5.4	1.6
	4	66.1	62.3	5.4	2.9	5.0	3.0	0.9
	5	77.6	54.8	11.9	3.1	4.6	9.0	2.3
	6	57.7	69.9	0.0	0.0	11.0	7.8	2.7
	7	86.1	70.0	166.8	0.0	6.0	7.0	1.6
	8	82.11	68.0	320.5	0.0	10.0	8.4	2.0
	9	66.9	75.5	1100.1	0.0	30.0	7.4	2.2
	10	75.8	68.2	2241.5	94.9	15.0	7.1	1.8
	11	80.5	72.3	109.1	0.0	4.5	7.0	1.7
β-pinene	12	100.2	71.3	479.1	0.0	12.0	9.4	1.2
	13	126.3	76.5	0.0	0.0	20.0	5.2	0.5
	14	94.5	71.4	15.2	0.0	4.0	5.4	0.7
	15	109.1	75.4	80.6	0.0	5.0	8.0	1.0
	16	96.5	67.6	38.0	0.0	5.0	7.9	1.1
	17	99.7	68.9	168.9	0.0	7.0	5.5	0.7
	18	73.6	77.2	341.4	0.0	7.5	6.9	1.2
	19	73.7	76.4	52.2	0.0	4.0	7.5	1.4
	20	85.9	75.0	1253.1	0.0	20.0	9.0	1.4
	21	69.6	115.4	2773.0	0.0	20.0	6.5	1.2

679

680

681 Table S 2. Boltzmann averaged dipole moments (μ) and lowest-energy conformer polarizability
682 (α) and derived collision rate (k) and CIMS sensitivity (c) of α-pinene (AN1-AN10) and β-pinene
683 (BN1-BN5) hydroxy nitrate isomers. The structures of hydroxy nitrate isomers are shown in
684 Scheme S 2. Dipole moments and polarizabilities are calculated at the B3LYP/cc-pVTZ level of
685 theory.

Isomer symbol	Dipole moment μ(D)	Polarizability α (Å^3)	Collision rate k (10^{-9} cm^3 molec^{-1} s^{-1})	Sensitivity c (10^{-4} ncts pptv^{-1})
AN1	3.5	21	2.6	2.0
AN2	3.5	20	2.6	1.9
AN3	2.8	20	2.2	1.7
AN4	3.4	20	2.5	1.9
AN5	2.9	20	2.3	1.7
AN6	2.8	20	2.2	1.7
AN7	2.7	20	2.2	1.6
AN8	3.0	20	2.3	1.8
AN9	3.2	20	2.4	1.8
AN10	3.4	21	2.5	1.9
BN1	3.0	20	2.3	1.8
BN2	2.9	20	2.3	1.7
BN3	3.2	20	2.4	1.8
BN4	3.2	20	2.4	1.8
BN5	3.4	21	2.5	1.9

686

687

688 Table S 3. Boltzmann averaged dipole moments (μ) and lowest-energy conformer polarizability
689 (α) and derived collision rate (k) and CIMS sensitivity (c) of α-pinene and β-pinene hydroxy
690 hydroperoxide isomers derived from the RO$_2$ A1-A10 and B1-B5 (Scheme S 2). Dipole moments
691 and polarizabilities are calculated at the B3LYP/cc-pVTZ level of theory.

Parent peroxy radical	Dipole moment μ(D)	Polarizability α (Å^3)	Collision rate k (10^{-9} cm^3 molec^{-1} s^{-1})	Sensitivity c (10^{-4} ncts pptv^{-1})
A1	2.0	19.0	1.9	1.4
A2	3.1	18.4	2.4	1.8
A3	1.4	18.5	1.6	1.2
A4	3.3	18.4	2.5	1.9
A5	1.5	18.5	1.7	1.3
A6	1.5	18.5	1.7	1.3
A7	3.3	18.4	2.5	1.9
A8	1.4	18.4	1.6	1.1
A9	3.1	18.4	2.4	1.8
A10	2.2	18.8	2.0	1.5
B1	2.8	18.4	2.2	1.7
B2	2.4	18.5	2.1	1.6
B3	2.8	18.3	2.2	1.7
B4	2.8	18.3	2.2	1.7
B5	2.1	19.1	1.9	1.5

692

693

694 Table S 4. Boltzmann averaged dipole moments (μ) and lowest-energy conformer polarizability
695 (α) of glycolaldehyde (calibration reference) and endoperoxide ketoaldehyde (P2 in Scheme 3,
696 main manuscript). All values are calculated at the B3LYP/cc-pVTZ level of theory. The sensitivity
697 of glycolaldehyde is an experimental value serving as the reference for the remaining compounds.

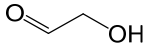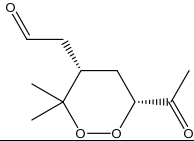| Compound	Dipole moment μ(D)	Polarizability α (Å^3)	Collision rate k (10^{-9} cm^3 molec^{-1} s^{-1})	Sensitivity c (10^{-4} ncts pptv^{-1})
	2.3	4.6	2.1	1.5
	3.3	19.0	2.5	1.9

698

699

700　Table S 5. Boltzmann averaged dipole moments (μ) and lowest-energy conformer polarizability
701　(α) and derived collision rate (k) and CIMS sensitivity (c) of α-pinene hydroxy hydroperoxide
702　(OOH) and hydroxy nitrate (N) isomers derived from the RO2 A2-A4 (Scheme S 2) as well as
703　glycolaldehyde (calibration reference). Dipole moments and polarizabilities are calculated at the
704　B3LYP/aug-cc-pVTZ level of theory. The sensitivity of glycolaldehyde is an experimental value
705　serving as the reference for the remaining compounds.

Compound	Dipole moment μ(D)	Polarizability α (Å^3)	Collision rate k (10^{-9} cm^3 molec^{-1} s^{-1})	Sensitivity c (10^{-4} ncts pptv^{-1})
Glycolaldehyde	2.5	5.2	2.2	1.5
A2-OOH	3.2	19.2	2.5	1.7
A3-OOH	1.4	19.3	1.7	1.1
A4-OOH	3.5	19.2	2.6	1.8
AN2	3.8	20.9	2.8	1.9
AN3	3.0	20.9	2.4	1.6
AN4	3.7	21.1	2.7	1.8

706

707

708 Table S 6. Calculated MC-TST reaction rate coefficients at 298.15 K for the unimolecular reactions
709 of the hydroxy peroxy radicals formed from α-pinene + OH + O_2. Calculated using the approach
710 by Møller et al.[24] All values are calculated at the ωB97X-D/aug-cc-pVTZ level, except for
711 electronic energies of the lowest-energy conformers and IRC end-points, which are at the F12 level.
712 Tunneling is based on IRC end-points. The abstraction/addition site refer to the structures in Figure
713 S 16, with "-OH" referring to abstraction of the hydrogen from the hydroxy group on the specified
714 carbon atom. The peroxy radicals are defined in Scheme S 2.

Peroxy radical	H-shift type	Abstraction/addition site	k (s^{-1})
A1	1,5 H-shift	G	1.1
	1,5 H-shift	D	$1.2 \cdot 10^{-6}$
	1,6 H-shift	E	0.37
	6-membered endoperoxide formation	A	0.35
	7-membered endoperoxide formation	F	$2.0 \cdot 10^{-3}$
A2	1,5-OH H-shift	E-OH	-
A4	1,5-OH H-shift	F-OH	-
A7	1,5-OH H-shift	F-OH	-
A9	1,5-OH H-shift	E-OH	-
A10	1,5 H-shift	G	0.16
	1,5 H-shift	D	$8.8 \cdot 10^{-6}$
	1,7-OH H-shift	E-OH	-
	6-membered endoperoxide formation	A	2.3
	7-membered endoperoxide formation	F	$2.6 \cdot 10^{-2}$

715

716

Table S 7. Calculated MC-TST reaction rate coefficients at 298.15 K for the unimolecular reactions of the hydroxy peroxy radicals formed from β-pinene + OH + O_2. Calculated using the approach by Møller et al.[24] All values are calculated at the ωB97X-D/aug-cc-pVTZ level, except for electronic energies of the lowest-energy conformers and IRC end-points, which are at the F12 level. Tunneling is based on IRC end-points. The abstraction/addition site refer to the structures in Figure S 17, with "-OH" referring to abstraction of the hydrogen from the hydroxy group on the specified carbon atom. The peroxy radicals are defined in Scheme S 2.

Peroxy radical	Reaction type	Abstraction/addition site	k (s^{-1})
B1	1,5-OH H-shift	F-OH	-
B2	1,5 H-shift	E	$8.1 \cdot 10^{-2}$
B2	1,5-OH H-shift	F-OH	-
B3	1,5-OH H-shift	J-OH	-
B4	1,5-OH H-shift	J-OH	-
B5	1,5 H-shift	G	1.4
B5	1,5 H-shift	D	$7.3 \cdot 10^{-6}$
B5	1,6 H-shift	E	$2.8 \cdot 10^{-1}$
B5	6-membered Endoperoxide formation	A	4.0
B5	7-membered Endoperoxide formation	F	$4.8 \cdot 10^{-2}$

726   Table S 8. Calculated MC-TST reaction rate coefficients at 298.15 K for the unimolecular reactions
727   of the hydroxy peroxy radicals formed from α-pinene + OH + O_2. All values are calculated at the
728   ωB97X-D/aug-cc-pVTZ level of theory with tunneling based on IRC end-points. The
729   abstraction/addition site refer to the structures in Figure S 16, with "-OH" referring to abstraction
730   of the hydrogen from the hydroxy group on the specified carbon atom. The peroxy radicals are
731   defined in Scheme S 2.

Peroxy radical	H-shift type	Abstraction/addition site	k (s^{-1})
A1	1,5 H-shift	G	0.66^a
	1,5 H-shift	D	$3.0 \cdot 10^{-7}$
	1,6 H-shift	E	0.96^a
	6-membered endoperoxide formation	A	$7.9 \cdot 10^{-2\ a}$
	7-membered endoperoxide formation	F	$1.1 \cdot 10^{-4}$
A2	1,5-OH H-shift	E-OH	$4.7 \cdot 10^{-2}$
A4	1,5-OH H-shift	F-OH	$2.8 \cdot 10^{-2}$
A7	1,5-OH H-shift	F-OH	$1.2 \cdot 10^{-2}$
A9	1,5-OH H-shift	E-OH	0.12
A10	1,5 H-shift	G	0.41
	1,5 H-shift	D	$8.3 \cdot 10^{-7}$
	1,7-OH H-shift	E-OH	$1.9 \cdot 10^{-9}$
	6-membered endoperoxide formation	A	0.95
	7-membered endoperoxide formation	F	$1.9 \cdot 10^{-3}$

732   [a] Also reported in Berndt et al.[43]

733

734

Table S 9. Calculated reaction rate coefficients at 298.15 K for the unimolecular reactions of the hydroxy peroxy radicals formed from β-pinene + OH + O_2. All values are calculated at the ωB97X-D/aug-cc-pVTZ level of theory with tunneling based on IRC end-points. The abstraction/addition site refer to the structures in Figure S 17, with "-OH" referring to abstraction of the hydrogen from the hydroxy group on the specified carbon atom. The peroxy radicals are defined in Scheme S 2.

Peroxy radical	Reaction type	Abstraction/addition site	k (s^{-1})
B1	1,5-OH H-shift	F-OH	$5.3 \cdot 10^{-4}$
B2	1,5 H-shift	E	$1.9 \cdot 10^{-2}$
	1,5-OH H-shift	F-OH	$1.6 \cdot 10^{-2}$
B3	1,5-OH H-shift	J-OH	$2.6 \cdot 10^{-4}$
B4	1,5-OH H-shift	J-OH	$1.8 \cdot 10^{-3}$
B5	1,5 H-shift	G	0.63
	1,5 H-shift	D	$2.7 \cdot 10^{-6}$
	1,6 H-shift	E	0.13
	6-membered Endoperoxide formation	A	0.34
	7-membered Endoperoxide formation	F	$1.5 \cdot 10^{-3}$

742　Table S 10. Calculated reaction rate coefficients at 298.15 K for the unimolecular reactions of the
743　hydroxy peroxy radicals formed from α-pinene + OH + O_2. All values are calculated at the
744　B3LYP/6-31+G(d) level of theory with tunneling assuming thermoneutral reactions. The
745　abstraction/addition site refer to the structures in Figure S 16, with "-OH" referring to abstraction
746　of the hydrogen from the hydroxy group on the specified carbon atom. The peroxy radicals are
747　defined in Scheme S 2. The reactions highlighted in bold are the ones also treated at a higher level
748　of theory.

Peroxy radical	Reaction type	Abstraction/addition site	k (s^{-1})
A1	**1,5 H-shift**	**G**	**63**
	1,5 H-shift	**D**	**1.8·10^{-4}**
	1,6 H-shift	**E**	**52**
	1,6 H-shift	A	3.5·10^{-17}
	1,7-OH H-shift	E-OH	9.4·10^{-16}
	6-membered endoperoxide formation	**A**	**2.7**
	7-membered endoperoxide formation	**F**	**1.7·10^{-3}**
A2	1,4 H-shift	A	2.9·10^{-10}
	1,5 H-shift	D	8.5·10^{-15}
	1,4 H-shift	E	5.8·10^{-20}
	1,5-OH H-shift	**E-OH**	**2.1**
	1,5 H-shift	G	3.6·10^{-3}
	1,4 H-shift	J	8.2·10^{-9}
A3	1,4 H-shift	A	6.0·10^{-11}
	1,5 H-shift	D	8.0·10^{-19}
	1,4 H-shift	E	5.1·10^{-4}
	1,5-OH H-shift	E-OH	2.2·10^{-7}
	1,6 H-shift	I	1.1·10^{-7}
	1,4 H-shift	J	1.3·10^{-9}
A4	1,4 H-shift	D	2.8·10^{-7}
	1,5-OH H-shift	**F-OH**	**7.4**
	1,6 H-shift	G	1.2·10^{-7}
A5	1,4 H-shift	D	4.3·10^{-8}
	1,5 H-shift	J	5.0·10^{-5}
	1,5-OH H-shift	F-OH	1.9·10^{-5}
	1,7 H-shift	I	5.0·10^{-8}
A6	1,4 H-shift	D	3.1·10^{-7}
	1,5 H-shift	J	4.7·10^{-5}
	1,5-OH H-shift	F-OH	5.3·10^{-6}
	1,6 H-shift	G	7.1·10^{-8}
A7	1,4 H-shift	D	1.4·10^{-8}

	1,5 H-shift	J	$2.9 \cdot 10^{-8}$
	1,5-OH H-shift	**F-OH**	**3.5**
	1,7 H-shift	I	$2.7 \cdot 10^{-6}$
A8	1,4 H-shift	A	$1.3 \cdot 10^{-10}$
	1,5 H-shift	D	$1.2 \cdot 10^{-19}$
	1,4 H-shift	E	$1.9 \cdot 10^{-3}$
	1,5-OH H-shift	E-OH	$6.5 \cdot 10^{-7}$
	1,5 H-shift	G	$1.3 \cdot 10^{-10}$
	1,4 H-shift	J	$2.5 \cdot 10^{-9}$
A9	1,4 H-shift	A	$1.2 \cdot 10^{-11}$
	1,5 H-shift	D	$6.4 \cdot 10^{-16}$
	1,4 H-shift	E	$2.8 \cdot 10^{-23}$
	1,5-OH H-shift	**E-OH**	**75**
	1,6 H-shift	I	$1.6 \cdot 10^{-4}$
	1,4 H-shift	J	$8.9 \cdot 10^{-10}$
A10	**1,5 H-shift**	**G**	**2.5**
	1,5 H-shift	**D**	**$6.9 \cdot 10^{-6}$**
	1,7-OH H-shift	**E-OH**	**$5.2 \cdot 10^{-5}$**
	6-membered endoperoxide formation	**A**	**20**
	7-membered endoperoxide formation	**F**	**$3.1 \cdot 10^{-2}$**

749

750

751 Table S 11. Calculated reaction rate coefficients at 298.15 K for the unimolecular reactions of the
752 hydroxy peroxy radicals formed from β-pinene + OH + O_2. All values are calculated at the
753 B3LYP/6-31+G(d) level of theory with tunneling assuming thermoneutral reactions. The
754 abstraction/addition site refer to the structures in Figure S 17, with "-OH" referring to abstraction
755 of the hydrogen from the hydroxy group on the specified carbon atom. The peroxy radicals are
756 defined in Scheme S 2. The reactions highlighted in bold are the ones also treated at a higher level
757 of theory.

Peroxy radical	Reaction type	Abstraction/addition site	k (s^{-1})
B1	1,5 H-shift	A	$5.1 \cdot 10^{-4}$
	1,6 H-shift	D	$6.1 \cdot 10^{-15}$
	1,5 H-shift	E	$1.6 \cdot 10^{-3}$
	1,5-OH H-shift	**F-OH**	**0.61**
	1,7 H-shift	I	$1.1 \cdot 10^{-4}$
B2	1,5 H-shift	A	$4.8 \cdot 10^{-4}$
	1,6 H-shift	D	$2.7 \cdot 10^{-11}$
	1,5 H-shift	**E**	**$1.9 \cdot 10^{-2}$**
	1,5-OH H-shift	**F-OH**	**22**
	1,6 H-shift	G	$5.2 \cdot 10^{-6}$
B3	1,4 H-shift	A	$6.3 \cdot 10^{-11}$
	1,5 H-shift	D	$4.4 \cdot 10^{-19}$
	1,4 H-shift	E	$1.9 \cdot 10^{-6}$
	1,5 H-shift	G	$2.4 \cdot 10^{-5}$
	1,4 H-shift	J	$6.3 \cdot 10^{-4}$
	1,5-OH H-shift	**J-OH**	**0.81**
B4	1,4 H-shift	A	$2.4 \cdot 10^{-5}$
	1,5 H-shift	D	$3.2 \cdot 10^{-17}$
	1,4 H-shift	E	$5.1 \cdot 10^{-7}$
	1,6 H-shift	I	$4.3 \cdot 10^{-6}$
	1,4 H-shift	J	$7.0 \cdot 10^{-4}$
	1,5-OH H-shift	**J-OH**	**0.87**
B5	**1,5 H-shift**	**G**	**2.7**
	1,5 H-shift	**D**	**$8.7 \cdot 10^{-7}$**
	1,6 H-shift	**E**	**0.12**
	1,9-OH H-shift	J-OH	$3.3 \cdot 10^{-10}$
	6-membered endoperoxide formation	**A**	**8.3**
	7-membered endoperoxide formation	**F**	**$2.7 \cdot 10^{-2}$**

758

759

760 Table S 12. Imaginary frequency (v_{imag}, cm^{-1}) of the lowest-energy TS, reaction and IRC barriers
761 (kcal/mol), approximate Eckart tunneling coefficient calculated assuming a thermoneutral reaction
762 ($\kappa_{thermoneutral}$) and Eckart tunneling coefficients calculated using the optimized IRC end-points
763 (κ_{IRC}). Values are given for the unimolecular reactions of the B5 peroxy radical. All values are
764 calculated using B3LYP/6-31+G(d). The abstraction/addition site refer to the structures in Figure
765 S 17.

Reaction	Abstraction/ addition site	v_{imag}	Reaction barrier[1]	Forward IRC barrier	Reverse IRC barrier	$\kappa_{thermoneutral}$[2]	κ_{IRC}[3]
1,5 H-shift	G	1819i	17.84	16.33	13.39	173.44	99.80
1,5 H-shift	D	1676i	25.72	24.42	4.58	164.19	10.72
1,6 H-shift	E	1738i	18.92	13.61	10.40	118.97	41.82
1,9-OH H-shift	J-OH	1322i	27.98	22.67	3.52	13.13	4.39
6-membered endoperoxide formation	A	492i	13.49	8.93	8.36	1.29	1.29
7-membered endoperoxide formation	F	448i	16.53	11.97	7.79	1.23	1.23

766 [1] Energy difference (Ee+ZPVE) between lowest-energy reactant and TS conformer

767 [2] Eckart tunneling coefficient calculated using the imaginary frequency and assuming both the forward and reverse

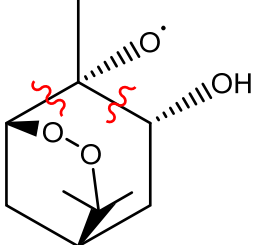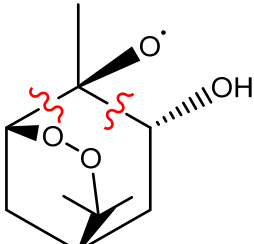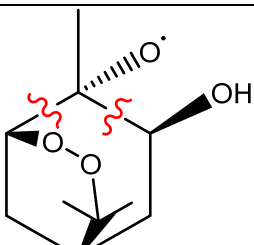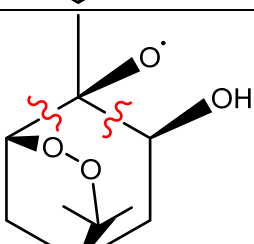768 IRC barriers are equal to the reaction barrier of the forward reaction.

769 [3] Eckart tunneling coefficient calculated using the imaginary frequency and the forward and reverse barriers obtained

770 from optimized end-points of the forward and reverse IRC from the lowest-energy TS.
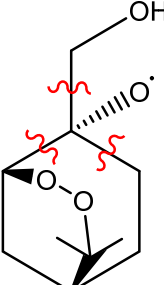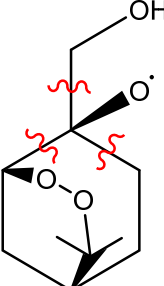
771

772

773

774 Table S 13. ωB97X-D/aug-cc-pVTZ calculated barrier heights (electronic energy and zero-point
775 correction, kcal/mol) between lowest-energy conformers for the possible bond scission pathways
776 of α-pinene R2 (Scheme 3, main manuscript).

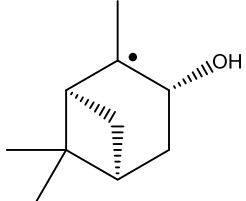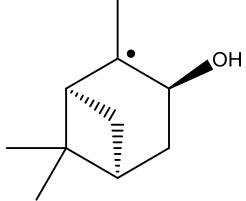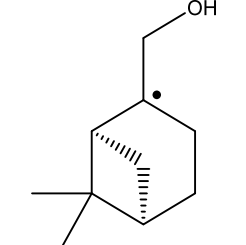| Isomer	Breaking towards -OO (left)	Breaking towards OH (right)
	6.2	3.0
	7.3	3.9
	6.5	2.8
	3.4	3.4

777

778

779   Table S 14. ωB97X-D/aug-cc-pVTZ calculated barrier heights (electronic energy and zero-point
780   correction, kcal/mol) between lowest-energy conformers for the possible bond scission pathways
781   of β-pinene R1 (Scheme S 6).

Isomer	Bond scission towards -OO (left)	Bond scission towards CH_2 (right)	Bond scission towards CH_2OH (up)
	2.8	8.9	6.2
	4.5	9.8	7.2

782

783

784　Table S 15. Structures formed by OH-addition to α-pinene and β-pinene of the three hydroxy alkyl
785　radicals which may potentially ring-open. For each, the amount of excess energy relative to the
786　free reactants, the barrier for ring-opening, the calculated canonical MC-TST rate coefficient and
787　the fraction ring-opening and adding O_2 is given. Electronic energies for the important species are
788　calculated using F12 and all other values using ωB97X-D/aug-cc-pVTZ.

Name	Structure	Excess energy (kcal/mol)	Barrier (kcal/mol)	Canonical rate coefficients (s^{-1})	Fraction ring-opening	Fraction adding O_2
α-pinene-OH I		27.96	13.29	9.9×10^2	0.33	0.67
α-pinene-OH II		27.53	13.20	5.5×10^2	0.31	0.69
β-pinene-OH		27.45	12.89	2.2×10^3	0.44	0.56

789

790

791 Table S 16. Reaction parameters of the three hydroxy alkyl radicals formed by OH-addition to α-
792 pinene and β-pinene which may potentially ring-open. For each, the amount of excess energy
793 relative to the free reactants, the barrier for ring-opening, the calculated canonical MC-TST rate
794 coefficient and the fraction ring-opening and adding O_2 is given. All values are calculated using
795 ωB97X-D/aug-cc-pVTZ.

Name	Excess energy (kcal/mol)	Barrier (kcal/mol)	Canonical rate coefficients (s^{-1})	Fraction ring-opening	Fraction adding O_2
α-pinene-OH I	31.16	14.47	6.4×10^1	0.24	0.76
α-pinene-OH II	30.59	14.21	1.0×10^2	0.25	0.75
β-pinene-OH	30.54	13.90	1.7×10^2	0.37	0.63

796

797

798   Table S 17. Fraction ring-opening before O_2-addition with the ring-opening barrier height changed
799   by ±1 kcal/mol. Everything else is as in Table S 15.

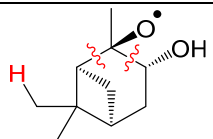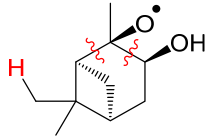| Name	Barrier -1 kcal/mol	Barrier +1 kcal/mol
α-pinene-OH I	0.59	0.15
α-pinene-OH II	0.57	0.15
β-pinene-OH	0.71	0.23

800

801

802   Table S 18. Fraction ring-opening before O_2-addition with the energy transfer per collision (ΔE_{down})
803   either decreased or increased by 75 cm^{-1}. Everything else is as in Table S 15.

Name	$\Delta E_{down} = 150$ cm^{-1}	$\Delta E_{down} = 300$ cm^{-1}
α-pinene-OH I	0.49	0.24
α-pinene-OH II	0.47	0.23
β-pinene-OH	0.62	0.34

804

805

806   Table S 19. MC-TST reaction rate coefficients (s^{-1}) for three competing reactions of two ring-
807   retained α-pinene hydroxy alkoxy radicals. The barrier height is calculated using either ωB97X-
808   D/aug-cc-pVTZ or F12 and all other values are calculated using ωB97X-D/aug-cc-pVTZ. Includes
809   an Eckart tunneling correction for all reactions. This H-shift reaction is possible only for the
810   isomers which have the alkoxy radical on the same side of the ring as the methyl groups on the
811   four-membered ring and the H-shift can only occur from the methyl group pointing towards the
812   alkoxy radical.

	Theory for barrier height	1,5 H-shift	Bond scission towards 4-membered ring (left)	Bond scission towards OH-group (right)
	ωB97X-D	2.1×10^8	9.1×10^5	6.2×10^{10}
	F12	1.9×10^8	-	3.5×10^8
	ωB97X-D	4.2×10^8	6.5×10^4	2.1×10^9
	F12	1.9×10^8	-	3.5×10^8

813
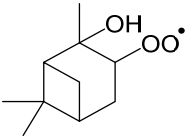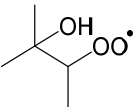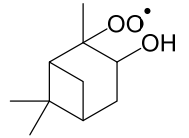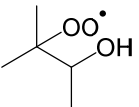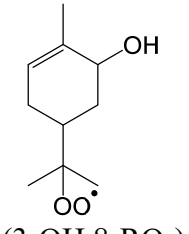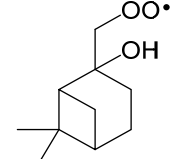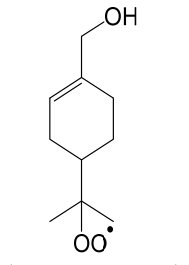
814

815   Table S 20. The signals of even mass between 200 and 360 relative to m/z 300 in an α-pinene
816   experiment with $\tau_{bimolecular}$ ~0.004 s^{-1}. Only m/z with signal accounting for more than 1% of that of
817   m/z 300 is included in the table. The isotope abundance of major odd mass (253, 269, and 285) has
818   been subtracted from relevant m/z's (254, 270, and 286).

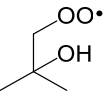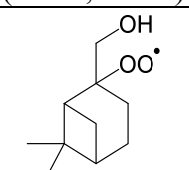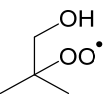| m/z	Signal relative to m/z 300	m/z	Signal relative to m/z 300
300	1.00	282	0.02
316	0.25	264	0.02
330	0.13	216	0.02
302	0.13	304	0.02
286	0.11	246	0.02
318	0.10	270	0.02
298	0.09	212	0.02
314	0.09	278	0.02
258	0.08	210	0.02
274	0.05	332	0.02
262	0.05	242	0.02
254	0.04	260	0.01
256	0.04	202	0.01
222	0.04	320	0.01
248	0.03	346	0.01
288	0.03	266	0.01
230	0.03	204	0.01
228	0.03	214	0.01
306	0.03	250	0.01
276	0.03	240	0.01
272	0.03	234	0.01
244	0.02	220	0.01

819

820   Table S 21. The estimated nitrate branching ratio (BR_{RONO2}) of α-pinene and β-pinene derived RO_2
821   under different assumptions.

RO_2	BR_{RONO2} (%) using calculated ring-opening fraction[a]	BR_{RONO2} (%) based on the same $BR_{RONO2,β-OH}$ assumption[b]	BR_{RONO2} (%) based on the different $BR_{RONO2,β-OH}$ assumption[c]	BR_{RONO2} (%) from Peeters et al.[d]	RO_2	BR_{RONO2} (%)[e]
(2-OH,3-RO₂)	3.1	9.2	8.2	7		5.4
(3-OH,2-RO₂)	0.7	9.2	10.2	3		11
(3-OH,8-RO₂)	10.8	2.2	2.3	11		
(2-OH,1-RO₂)	15.9	9.2	6.1			4.9
(1-OH,2-RO₂)	10.2	9.2	10.2			10
(1-OH,8-RO₂)	1.7	2.2	2.3			

822

823   [a]Assuming that $BR_{add\_C3} = 0.5$, $BR_{\alpha\text{-pinene,ring-open}} = 0.32$, $BR_{add\_C1} = 0.93$, and $BR_{\beta\text{-pinene,ring-open}} =$
824   0.44.

825   [b]Assuming that (1) the ring-opened RO_2 of both α-pinene and β-pinene have the same BR_{RONO2}
826   and (2) all the β-hydroxy RO_2 have the same BR_{RONO2}. See section S6 for details.

827   [c]Assuming that (1) the ring-opened RO_2 of both α-pinene and β-pinene have the same BR_{RONO2}
828   and (2) the ratio of BR_{RONO2} for tertiary, secondary, and primary β-hydroxy RO_2 is 1.25: 1: 0.75.
829   See section S6 for details.

830   [d]Peeters et al.[56] estimated based on structure-activity-relationship.

831   [e]The BR_{RONO2} of 2-methyl 2-butene and methylpropene RO_2, which share a similar structure but
832   different size as the substitutions on α-pinene and β-pinene C-C double bond, respectively. The
833   values are experimentally constrained by Teng et al.[2]

834

References

1. Kurtén, T.; Møller, K. H.; Nguyen, T. B.; Schwantes, R. H.; Misztal, P. K.; Su, L.; Wennberg, P. O.; Fry, J. L.; Kjaergaard, H. G. Alkoxy Radical Bond Scissions Explain the Anomalously Low Secondary Organic Aerosol and Organonitrate Yields from A-Pinene + No3. *J. Phys. Chem. Lett* **2017**, 2826-2834.

2. Teng, A. P.; Crounse, J. D.; Lee, L.; St. Clair, J. M.; Cohen, R. C.; Wennberg, P. O. Hydroxy Nitrate Production in the Oh-Initiated Oxidation of Alkenes. *Atmos. Chem. Phys.* **2015,** *15*, 4297-4316.

3. O'Haver Interactive Peak Fitter. *Available at https://terpconnect.umd.edu/~toh/spectrum/InteractivePeakFitter.htm.* **2016**.

4. Saunders, S. M.; Jenkin, M. E.; Derwent, R. G.; Pilling, M. J. Protocol for the Development of the Master Chemical Mechanism, Mcm V3 (Part a): Tropospheric Degradation of Non-Aromatic Volatile Organic Compounds. *Atmos. Chem. Phys.* **2003,** *3*, 161-180.

5. Crounse, J. D.; Paulot, F.; Kjaergaard, H. G.; Wennberg, P. O. Peroxy Radical Isomerization in the Oxidation of Isoprene. *Phys. Chem. Chem. Phys.* **2011,** *13*, 13607-13613.

6. Teng, A. P.; Crounse, J. D.; Wennberg, P. O. Isoprene Peroxy Radical Dynamics. *J. Am. Chem. Soc.* **2017,** *139*, 5367-5377.

7. Garden, A. L.; Paulot, F.; Crounse, J. D.; Maxwell-Cameron, I. J.; Wennberg, P. O.; Kjaergaard, H. G. Calculation of Conformationally Weighted Dipole Moments Useful in Ion–Molecule Collision Rate Estimates. *Chem Phys Lett* **2009,** *474*, 45-50.

8. Paulot, F.; Crounse, J. D.; Kjaergaard, H. G.; Kroll, J. H.; Seinfeld, J. H.; Wennberg, P. O. Isoprene Photooxidation: New Insights into the Production of Acids and Organic Nitrates. *Atmos. Chem. Phys.* **2009,** *9*, 1479-1501.

9. Crounse, J. D.; Paulot, F.; Kjaergaard, H. G.; Wennberg, P. O. Peroxy Radical Isomerization in the Oxidation of Isoprene. *Phys Chem Chem Phys* **2011,** *13*, 13607-13613.

10. Werner, H.-J.; Knizia, G.; Manby, F. R. Explicitly Correlated Coupled Cluster Methods with Pair-Specific Geminals. *Molecular Physics* **2011,** *109*, 407-417.

11. Halgren, T. A. Mmff Vii. Characterization of Mmff94, Mmff94s, and Other Widely Available Force Fields for Conformational Energies and for Intermolecular-Interaction Energies and Geometries. *Journal of Computational Chemistry* **1999,** *20*, 730-748.

12. Halgren, T. A. Merck Molecular Force Field. V. Extension of Mmff94 Using Experimental Data, Additional Computational Data, and Empirical Rules. *Journal of Computational Chemistry* **1996,** *17*, 616-641.

13. Halgren, T. A.; Nachbar, R. B. Merck Molecular Force Field. Iv. Conformational Energies and Geometries for Mmff94. *Journal of Computational Chemistry* **1996,** *17*, 587-615.

14. Halgren, T. A. Merck Molecular Force Field. Iii. Molecular Geometries and Vibrational Frequencies for Mmff94. *Journal of Computational Chemistry* **1996,** *17*, 553-586.

15. Halgren, T. A. Merck Molecular Force Field. Ii. Mmff94 Van Der Waals and Electrostatic Parameters for Intermolecular Interactions. *Journal of Computational Chemistry* **1996,** *17*, 520-552.

16. Halgren, T. A. Merck Molecular Force Field. I. Basis, Form, Scope, Parameterization, and Performance of Mmff94. *Journal of Computational Chemistry* **1996,** *17*, 490-519.

17. Frisch, M. J.; Trucks, G. W.; Schlegel, H. B.; Scuseria, G. E.; Robb, M. A.; Cheeseman, J. R.; Scalmani, G.; Barone, V.; Petersson, G. A.; Nakatsuji, H., et al. *Gaussian 16 Rev. A.03*, Wallingford, CT, 2016.

880   18.   Becke, A. D. Density-Functional Thermochemistry. Iii. The Role of Exact Exchange. *The*
881   *Journal of Chemical Physics* **1993,** *98*, 5648-5652.
882   19.   Lee, C.; Yang, W.; Parr, R. G. Development of the Colle-Salvetti Correlation-Energy
883   Formula into a Functional of the Electron Density. *Physical Review B* **1988,** *37*, 785-789.
884   20.   Hehre, W. J.; Ditchfield, R.; Pople, J. A. Self—Consistent Molecular Orbital Methods. Xii.
885   Further Extensions of Gaussian—Type Basis Sets for Use in Molecular Orbital Studies of Organic
886   Molecules. *The Journal of Chemical Physics* **1972,** *56*, 2257-2261.
887   21.   Clark, T.; Chandrasekhar, J.; Spitznagel, G. W.; Schleyer, P. V. R. Efficient Diffuse
888   Function-Augmented Basis Sets for Anion Calculations. Iii. The 3-21+G Basis Set for First-Row
889   Elements, Li–F. *Journal of Computational Chemistry* **1983,** *4*, 294-301.
890   22.   Frisch, M. J.; Pople, J. A.; Binkley, J. S. Self-Consistent Molecular Orbital Methods 25.
891   Supplementary Functions for Gaussian Basis Sets. *The Journal of Chemical Physics* **1984,** *80*,
892   3265-3269.
893   23.   Dunning Jr., T. H. Gaussian Basis Sets for Use in Correlated Molecular Calculations. I.
894   The Atoms Boron through Neon and Hydrogen. *The Journal of Chemical Physics* **1989,** *90*, 1007-
895   1023.
896   24.   Møller, K. H.; Otkjær, R. V.; Hyttinen, N.; Kurtén, T.; Kjaergaard, H. G. Cost-Effective
897   Implementation of Multiconformer Transition State Theory for Peroxy Radical Hydrogen Shift
898   Reactions. *J. Phys. Chem. A* **2016,** *120*, 10072-10087.
899   25.   *Spartan'16*, Wavefunction, Inc., Irvine, CA.
900   26.   Chai, J.-D.; Head-Gordon, M. Long-Range Corrected Hybrid Density Functionals with
901   Damped Atom-Atom Dispersion Corrections. *Physical Chemistry Chemical Physics* **2008,** *10*,
902   6615-6620.
903   27.   Kendall, R. A.; Dunning Jr., T. H.; Harrison, R. J. Electron Affinities of the First-Row
904   Atoms Revisited. Systematic Basis Sets and Wave Functions. *The Journal of Chemical Physics*
905   **1992,** *96*, 6796-6806.
906   28.   Adler, T. B.; Knizia, G.; Werner, H.-J. A Simple and Efficient Ccsd(T)-F12 Approximation.
907   *Accounts of Chemical Research* **2007,** *127*, 221106.
908   29.   Knizia, G.; Adler, T. B.; Werner, H.-J. Simplified Ccsd(T)-F12 Methods: Theory and
909   Benchmarks. *The Journal of Chemical Physics* **2009,** *130*, 054104.
910   30.   Peterson, K. A.; Adler, T. B.; Werner, H.-J. Systematically Convergent Basis Sets for
911   Explicitly Correlated Wavefunctions: The Atoms H, He, B–Ne, and Al–Ar. *The Journal of*
912   *Chemical Physics* **2008,** *128*, 084102.
913   31.   Watts, J. D.; Gauss, J.; Bartlett, R. J. Coupled-Cluster Methods with Noniterative Triple
914   Excitations for Restricted Open-Shell Hartree–Fock and Other General Single Determinant
915   Reference Functions. Energies and Analytical Gradients. *The Journal of Chemical Physics* **1993,**
916   *98*, 8718-8733.
917   32.   Werner, H.-J.; Knizia, G.; R. Manby, F. Explicitly Correlated Coupled Cluster Methods
918   with Pair-Specific Geminals. *Molecular Physics* **2011,** *109*, 407-417.
919   33.   Werner, H.-J.; Knowles, P. J.; Knizia, G.; Manby, F. R.; Schütz, M. Molpro: A General-
920   Purpose Quantum Chemistry Program Package. *Wiley Interdisciplinary Reviews: Computational*
921   *Molecular Science* **2012,** *2*, 242-253.
922   34.   Werner, H.-J.; Knowles, P. J.; Knizia, G.; Manby, F. R.; Schütz, M.; Celani, P.; Györffy,
923   W.; Kats, D.; Korona, T.; Lindh, R., et al. *Molpro, Version 2012.1, a Package of Ab Initio*
924   *Programs*, 2012.

35. Rienstra-Kiracofe, J. C.; Allen, W. D.; Schaefer, H. F. The C2h5 + O2 Reaction Mechanism: High-Level Ab Initio Characterizations. *The Journal of Physical Chemistry A* **2000,** *104*, 9823-9840.

36. Lambert, N.; Kaltsoyannis, N.; Price, S. D.; Žabka, J.; Herman, Z. Bond-Forming Reactions of Dications with Molecules: A Computational and Experimental Study of the Mechanisms for the Formation of Hcf2+ from Cf32+ and H2. *The Journal of Physical Chemistry A* **2006,** *110*, 2898-2905.

37. Jayatilaka, D.; Lee, T. J. Open-Shell Coupled-Cluster Theory. *The Journal of Chemical Physics* **1993,** *98*, 9734-9747.

38. Matlab R2016b.

39. Eckart, C. The Penetration of a Potential Barrier by Electrons. *Physical Review* **1930,** *35*, 1303-1309.

40. Evans, M. G.; Polanyi, M. Some Applications of the Transition State Method to the Calculation of Reaction Velocities, Especially in Solution. *Transactions of the Faraday Society* **1935,** *31*, 875-894.

41. Eyring, H. The Activated Complex and the Absolute Rate of Chemical Reactions. *Chemical Reviews* **1935,** *17*, 65-77.

42. Vereecken, L.; Peeters, J. The 1,5-H-Shift in 1-Butoxy: A Case Study in the Rigorous Implementation of Transition State Theory for a Multirotamer System. *The Journal of Chemical Physics* **2003,** *119*, 5159-5170.

43. Berndt, T.; Richters, S.; Jokinen, T.; Hyttinen, N.; Kurtén, T.; Otkjær, R. V.; Kjaergaard, H. G.; Stratmann, F.; Herrmann, H.; Sipilä, M., et al. Hydroxyl Radical-Induced Formation of Highly Oxidized Organic Compounds. *Nat. Commun.* **2016,** *7*, 13677.

44. Kurtén, T.; Møller, K. H.; Nguyen, T. B.; Schwantes, R. H.; Misztal, P. K.; Su, L.; Wennberg, P. O.; Fry, J. L.; Kjaergaard, H. G. Alkoxy Radical Bond Scissions Explain the Anomalously Low Secondary Organic Aerosol and Organonitrate Yields from A-Pinene + No3. *The Journal of Physical Chemistry Letters* **2017,** *8*, 2826-2834.

45. Glowacki, D. R.; Liang, C.-H.; Morley, C.; Pilling, M. J.; Robertson, S. H. Mesmer: An Open-Source Master Equation Solver for Multi-Energy Well Reactions. *J. Phys. Chem. A* **2012,** *116*, 9545-9560.

46. Chuong, B.; Davis, M.; Edwards, M.; Stevens, P. S. Measurements of the Kinetics of the Oh + A-Pinene and Oh + B-Pinene Reactions at Low Pressure. *International Journal of Chemical Kinetics* **2002,** *34*, 300-308.

47. Wu, D.; Bayes, K. D. Rate Constants for the Reactions of Isobutyl, Neopentyl, Cyclopentyl, and Cyclohexyl Radicals with Molecular Oxygen. *International Journal of Chemical Kinetics* **1986,** *18*, 547-554.

48. Allen, H. M.; Crounse, J. D.; Bates, K. H.; Teng, A. P.; Krawiec-Thayer, M. P.; Rivera-Rios, J. C.; Keutsch, F. N.; St. Clair, J. M.; Hanisco, T. F.; Møller, K. H., et al. Kinetics and Product Yields of the Oh Initiated Oxidation of Hydroxymethyl Hydroperoxide. *The Journal of Physical Chemistry A* **2018,** *122*, 6292-6302.

49. Forst, W. Analytic Solution of Relaxation in a System with Exponential Transition Probabilities. Iii. Macroscopic Disequilibrium. *The Journal of Chemical Physics* **1984,** *80*, 2504-2513.

50. Kurtén, T.; Rissanen, M. P.; Mackeprang, K.; Thornton, J. A.; Hyttinen, N.; Jørgensen, S.; Ehn, M.; Kjaergaard, H. G. Computational Study of Hydrogen Shifts and Ring-Opening

Mechanisms in A-Pinene Ozonolysis Products. *The Journal of Physical Chemistry A* **2015,** *119*, 11366-11375.

51.   Cuadros, F.; Cachadiña, I.; Ahumada, W. Determination of Lennard-Jones Interaction Parameters Using a New Procedure. *Molecular Engineering* **1996,** *6*, 319-325.

52.   Su, T.; Chesnavich, W. J. Parametrization of the Ion–Polar Molecule Collision Rate Constant by Trajectory Calculations. *The Journal of Chemical Physics* **1982,** *76*, 5183-5185.

53.   Atkinson, R.; Aschmann, S. M.; Carter, W. P. L.; Winer, A. M.; Pitts, J. N. Alkyl Nitrate Formation from the Nitrogen Oxide (Nox)-Air Photooxidations of C2-C8 N-Alkanes. *The Journal of Physical Chemistry* **1982,** *86*, 4563-4569.

54.   Eddingsaas, N. C.; Loza, C. L.; Yee, L. D.; Chan, M.; Schilling, K. A.; Chhabra, P. S.; Seinfeld, J. H.; Wennberg, P. O. A-Pinene Photooxidation under Controlled Chemical Conditions &Ndash; Part 2: Soa Yield and Composition in Low- and High-Nox Environments. *Atmos. Chem. Phys.* **2012,** *12*, 7413-7427.

55.   Bean, J. K.; Hildebrandt Ruiz, L. Gas–Particle Partitioning and Hydrolysis of Organic Nitrates Formed from the Oxidation of A-Pinene in Environmental Chamber Experiments. *Atmos. Chem. Phys.* **2016,** *16*, 2175-2184.

56.   Nozière, B.; Barnes, I.; Becker, K.-H. Product Study and Mechanisms of the Reactions of A-Pinene and of Pinonaldehyde with Oh Radicals. *Journal of Geophysical Research: Atmospheres* **1999,** *104*, 23645-23656.

57.   Cleaves, H. J., Branching Ratio. In *Encyclopedia of Astrobiology*, Gargaud, M.; Amils, R.; Quintanilla, J. C.; Cleaves, H. J.; Irvine, W. M.; Pinti, D. L.; Viso, M., Eds. Springer Berlin Heidelberg: Berlin, Heidelberg, 2011; pp 218-218.

58.   Peeters, J.; Vereecken, L.; Fantechi, G. The Detailed Mechanism of the Oh-Initiated Atmospheric Oxidation of A-Pinene: A Theoretical Study. *Phys. Chem. Chem. Phys.* **2001,** *3*, 5489-5504.

59.   Vereecken, L.; Peeters, J. Theoretical Study of the Formation of Acetone in the Oh-Initiated Atmospheric Oxidation of A-Pinene. *J. Phys. Chem. A* **2000,** *104*, 11140-11146.

60.   Wennberg, P. O.; Bates, K. H.; Crounse, J. D.; Dodson, L. G.; McVay, R. C.; Mertens, L. A.; Nguyen, T. B.; Praske, E.; Schwantes, R. H.; Smarte, M. D., et al. Gas-Phase Reactions of Isoprene and Its Major Oxidation Products. *Chem. Rev.* **2018,** *118*, 3337-3390.

61.   Vereecken, L.; Muller, J. F.; Peeters, J. Low-Volatility Poly-Oxygenates in the Oh-Initiated Atmospheric Oxidation of A-Pinene: Impact of Non-Traditional Peroxyl Radical Chemistry. *Phys. Chem. Chem. Phys.* **2007,** *9*, 5241-5248.

62.   Aschmann, S. M.; Atkinson, R.; Arey, J. Products of Reaction of Oh Radicals with A-Pinene. *J. Geophys. Res. - Atmos* **2002,** *107*, ACH 6-1-ACH 6-7.

63.   Wisthaler, A.; Jensen, N. R.; Winterhalter, R.; Lindinger, W.; Hjorth, J. Measurements of Acetone and Other Gas Phase Product Yields from the Oh-Initiated Oxidation of Terpenes by Proton-Transfer-Reaction Mass Spectrometry (Ptr-Ms). *Atmospheric Environ.* **2001,** *35*, 6181-6191.